Operational experience and aging studies on the CDF Run II Silicon Vertex Detectors

Benedetto Di Ruzza on behalf of the CDF II Silicon Operation Group

2nd International Conference on Technology and Instrumentation in Particle Physics

Chicago June 8th – 14th 2011

OUTLINE

1) The Tevatron
2) The CDF II detector
3) The CDF II silicon subdetectors
4) Silicon aging studies
5) Conclusions

The Tevatron and the CDFII detector

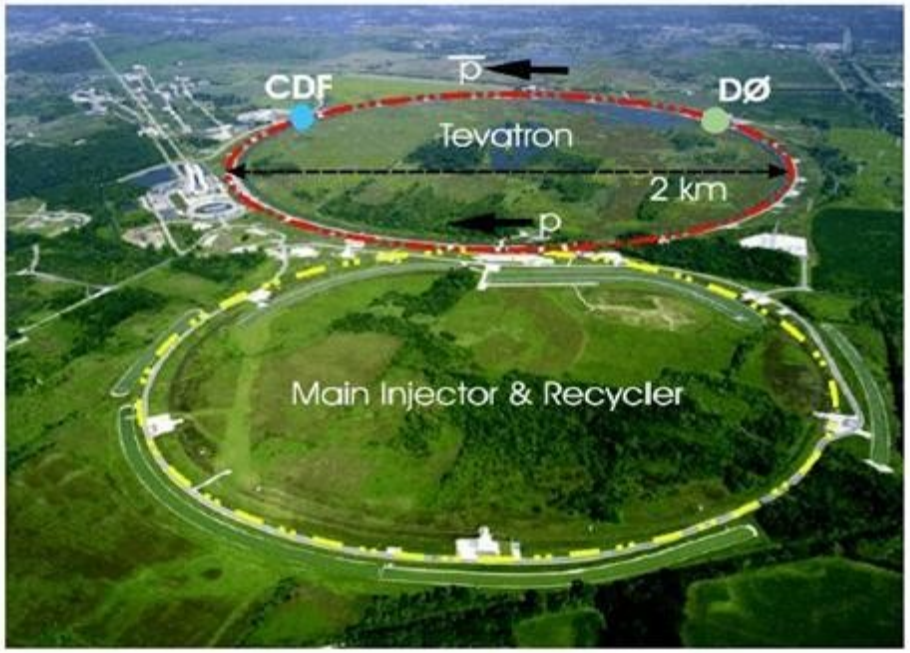

➢ **Tevatron:** proton-antiproton collider at $\sqrt{s} = 1.96$ TeV

Two multi-purpose detectors: CDF & DØ

➢ **CDF II:** Multilayered HEP detector with excellent tracking

- ✓ silicon detectors designed for ~3 fb^{-1}
- ✓ large open-cell drift chamber

Fermilab accelerators chain

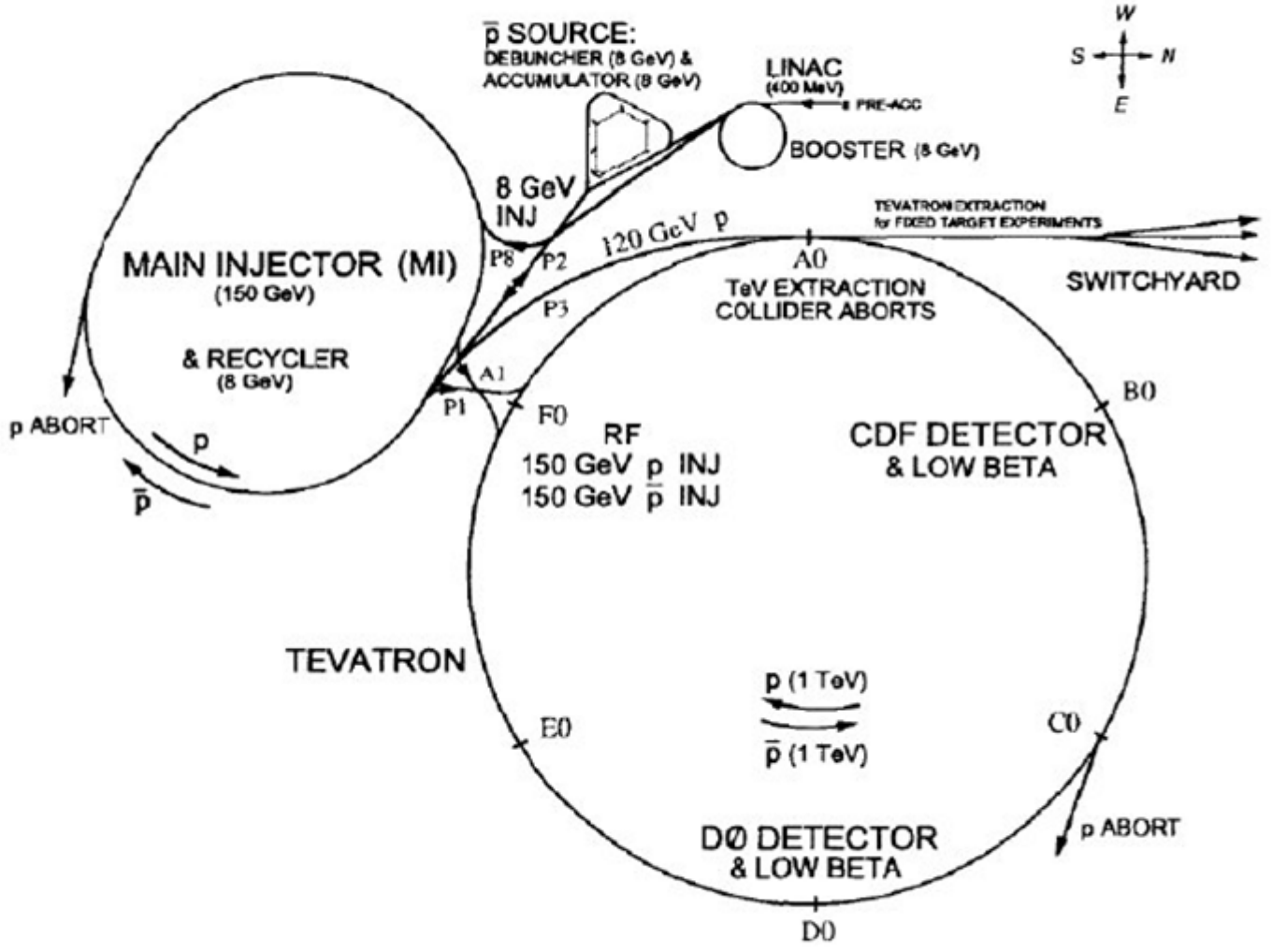

View of the accelerators chain

The Tevatron

Bunches structure

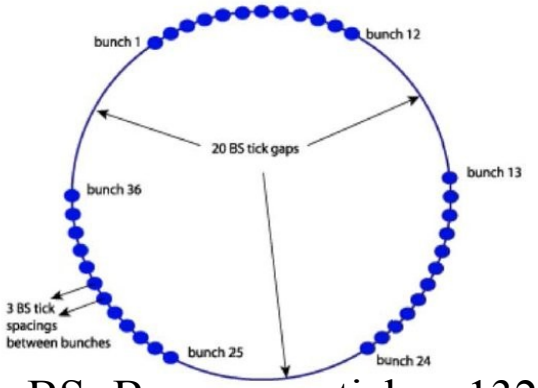

BS=Beam sync ticks =132ns

Initial luminosity record: 4.05 x10^{+32} (cm^{-2} s^{-1})

Mean Pbar production efficiency: ~ 22 x10^{-6}

Mean Pbar Accumulation rate: ~ 25x10^{+10} (hr^{-1})

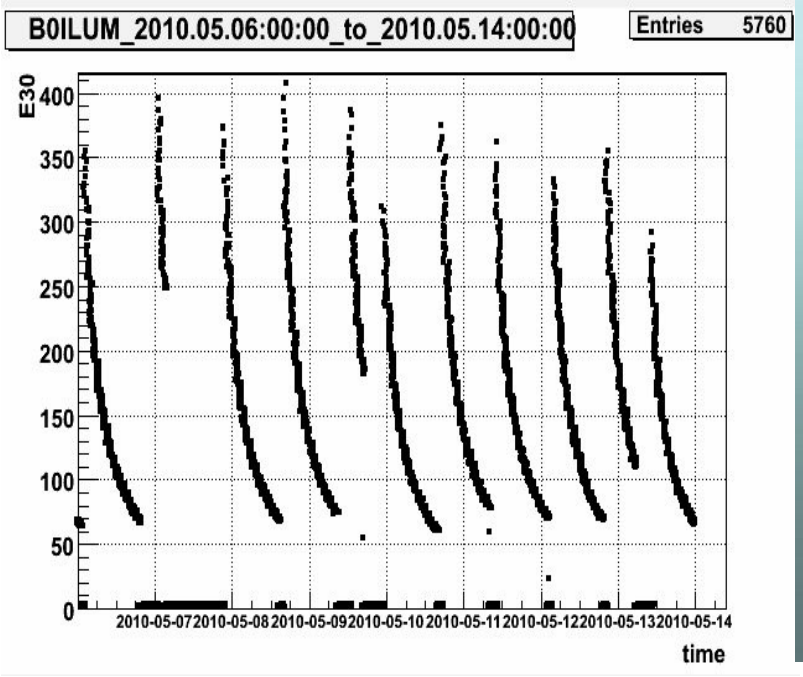

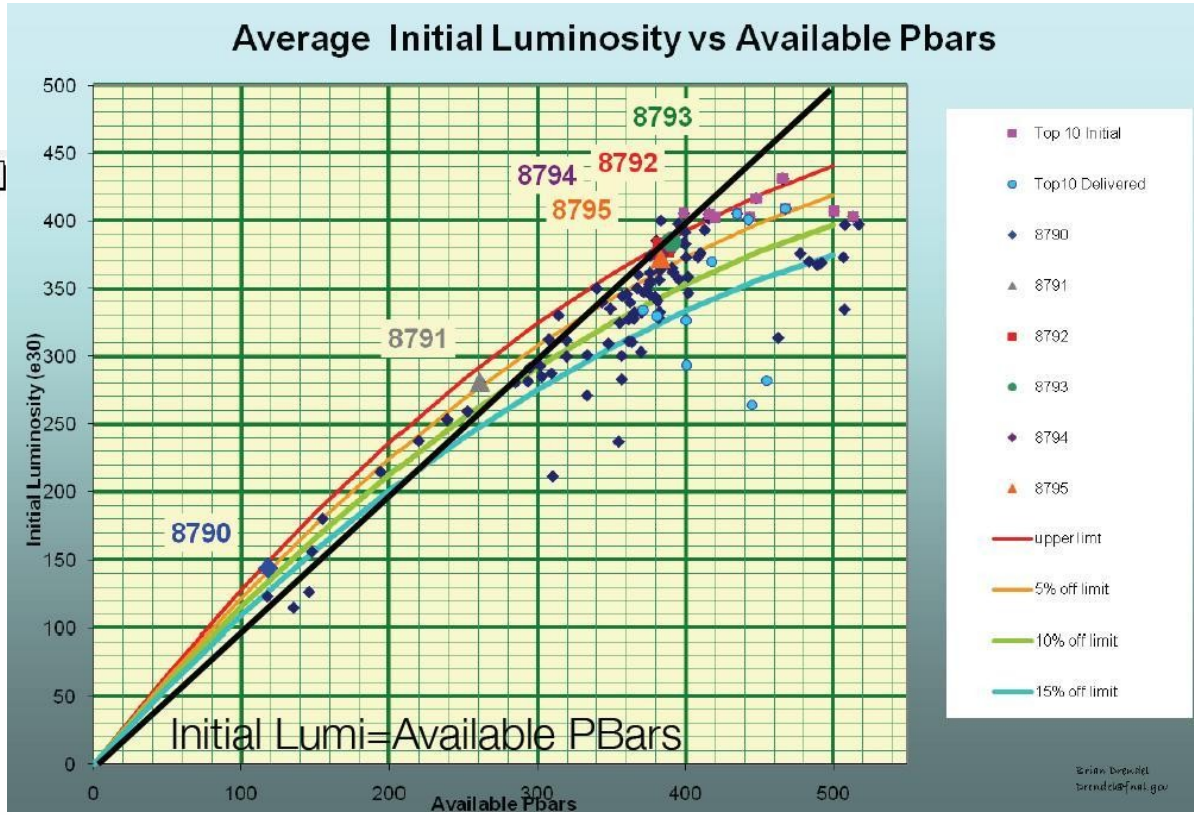

CDF Recorded Luminosity

- Two major milestones reached in the last month
  - 11.2 fb^{-1} delivered to CDF
  - 9.3 fb^{-1} recorded by CDF

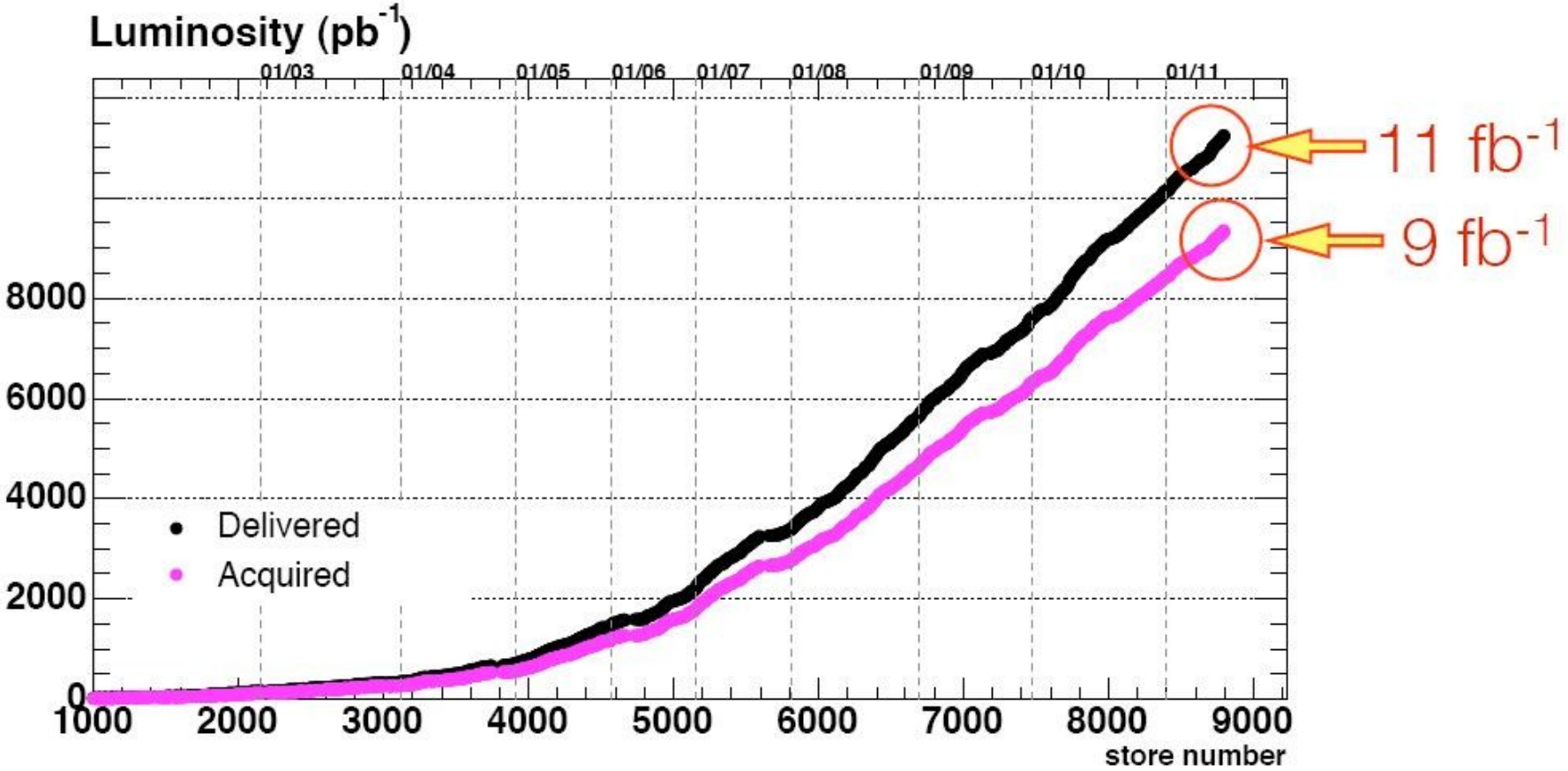

Dose rate during beam dump

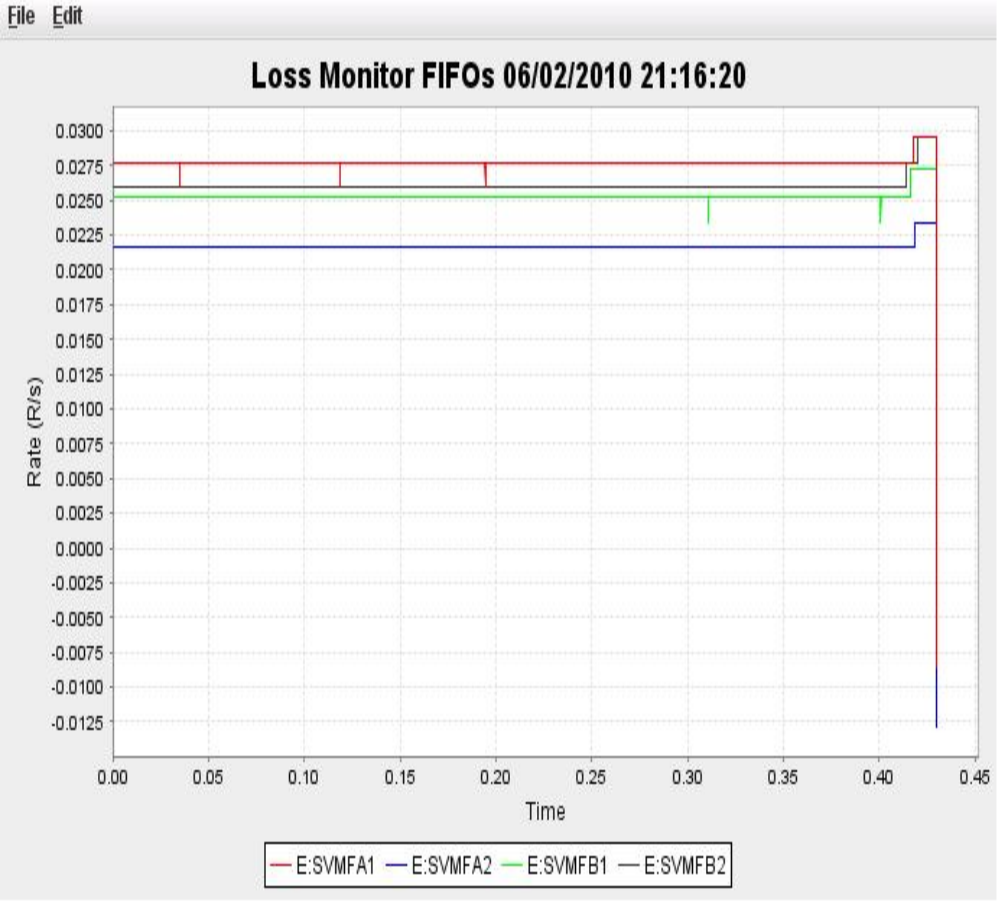

Clean abort

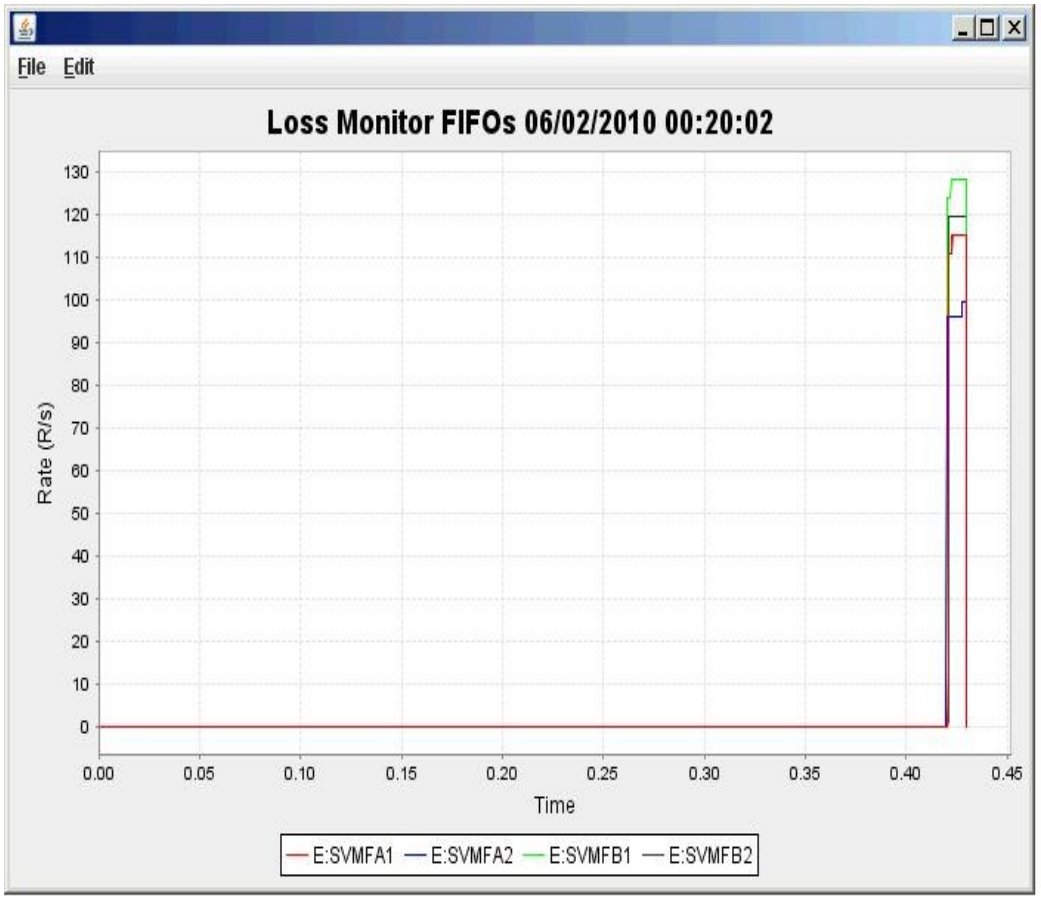

Quench

Dose rate during data taking

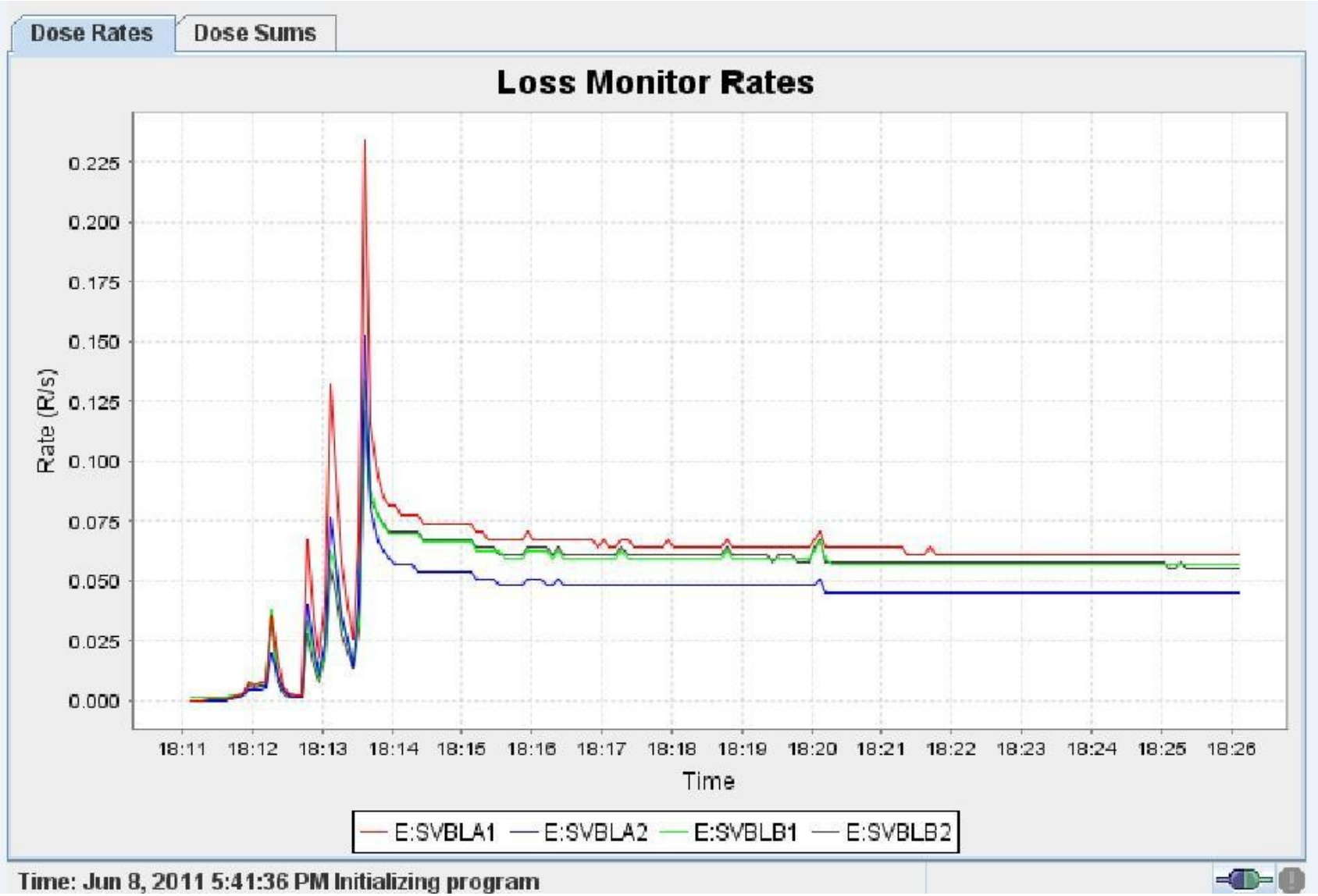

Beam doses during data taking

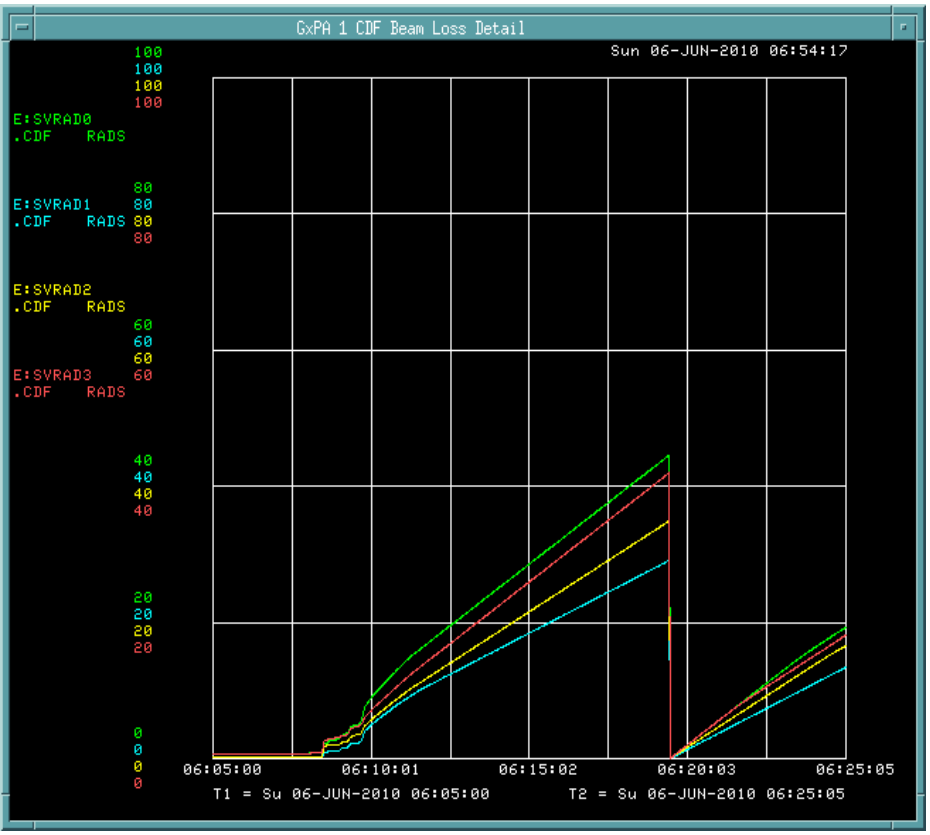

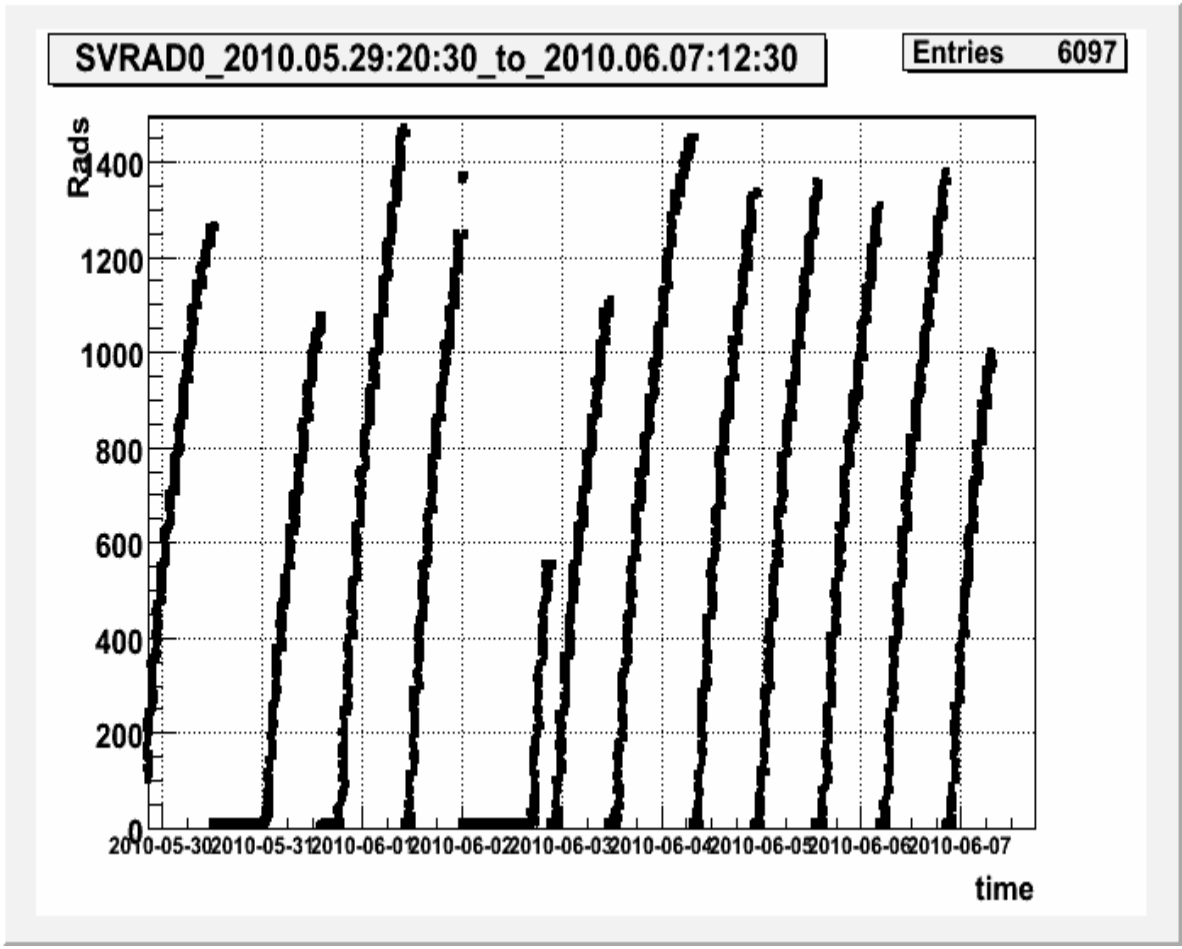

Beam condition during data taking

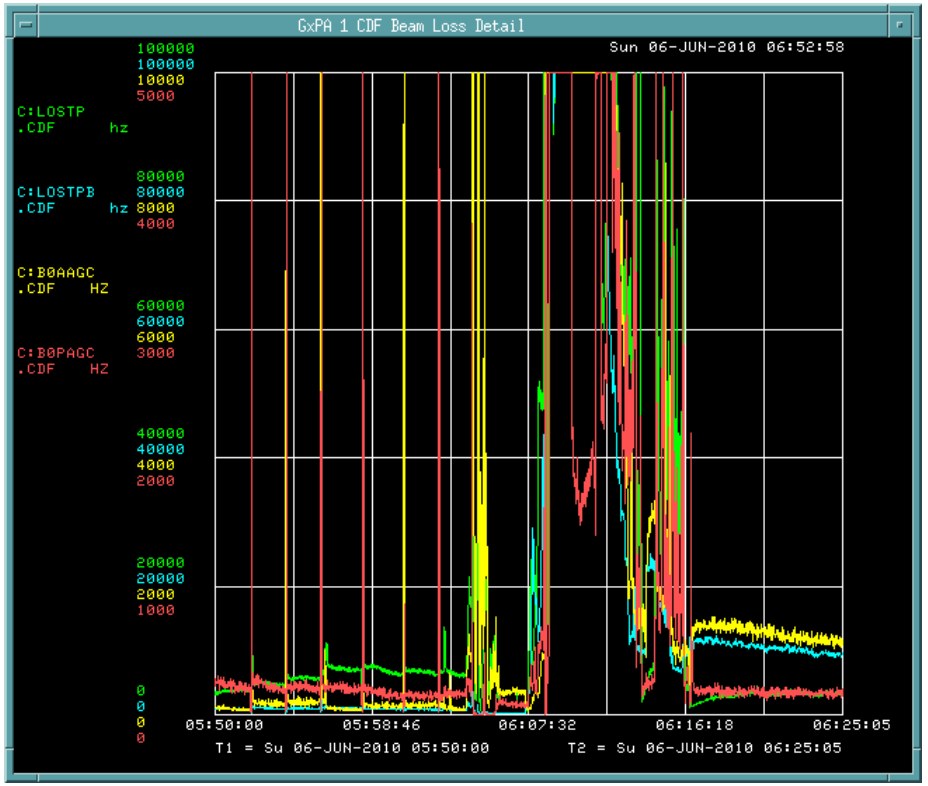

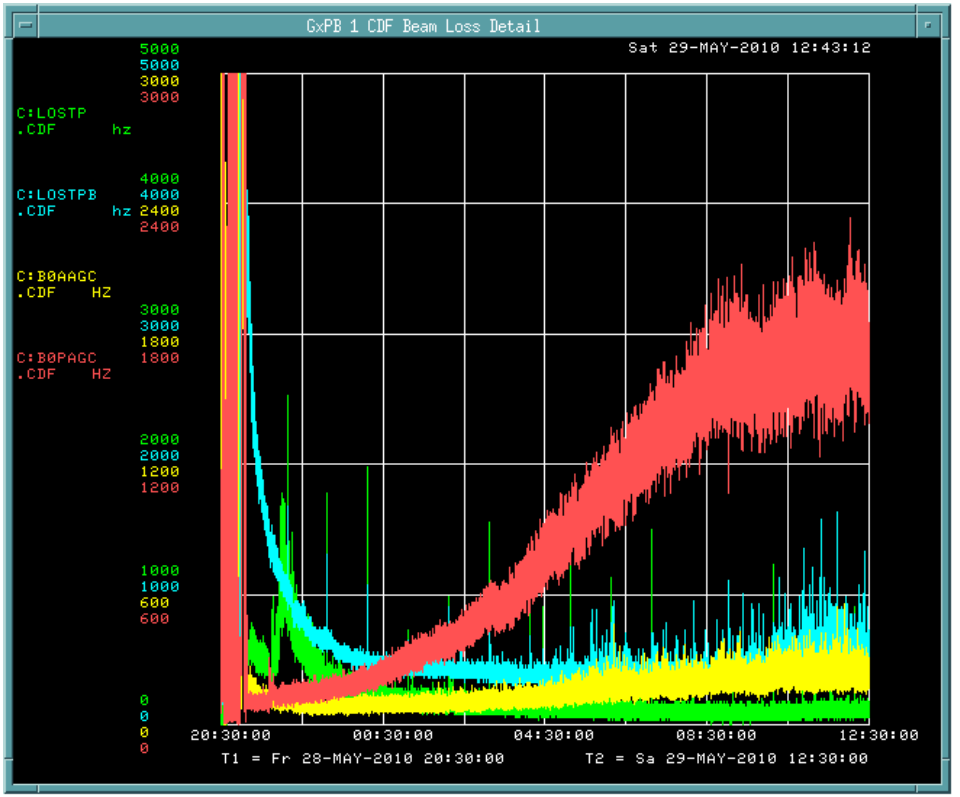

The CDFII Detector

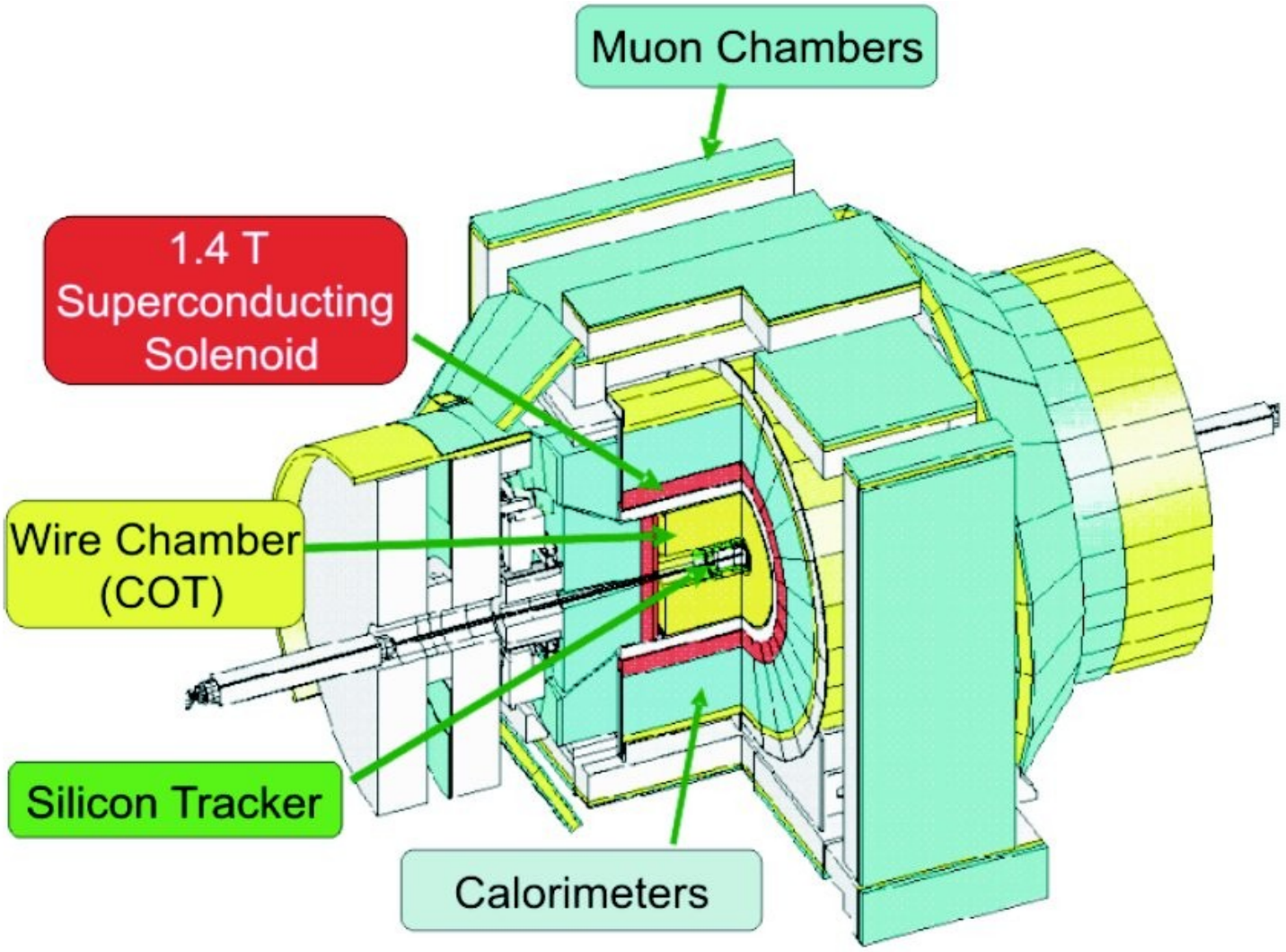

The Silicon Detectors

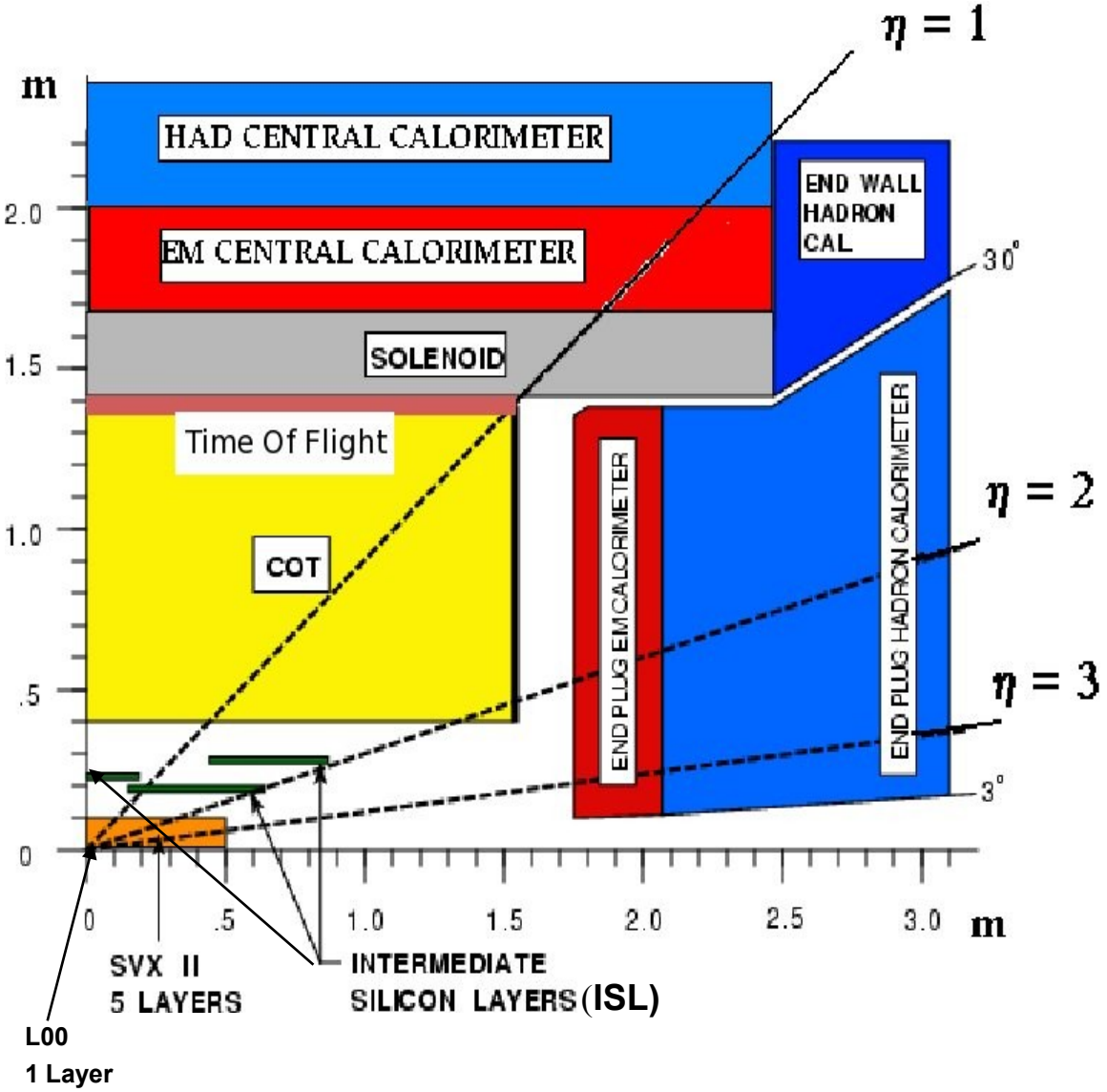

The CDFII Silicon detectors

OVERVIEW

L00: Single-sided strips: "Narrows" (SGS Thomson and 2 Microns)
"Wides" (Hamamatsu).

SVX: Double-sided strips: Layers 0,1,3 (Hamamatsu) perpendicular strips,
Layers 2,4 (Micron) small angled strips.

ISL: Double-sided strips: (Hamamatsu+Micron) small angled strips

The Silicon Detectors

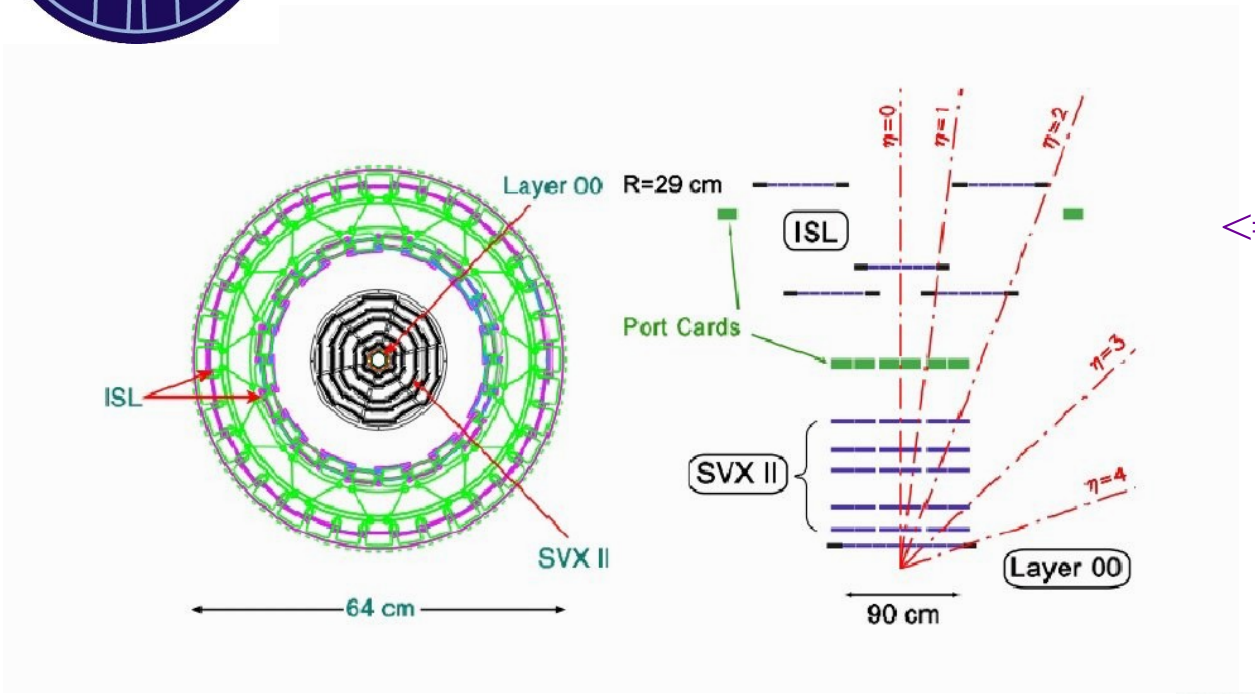

<== X-Y (r-phi) and Y-Z (r-z) views

L00 detail ==> narrow sensors

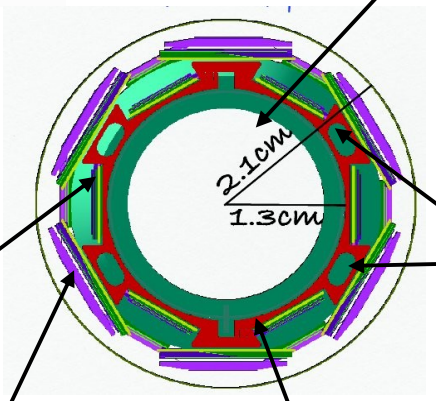

Beam pipe

Cooling lines

wide sensors

carbon support

The Silicon Detectors

SVXII detail:
3 barrels
5 layers
12 wedges

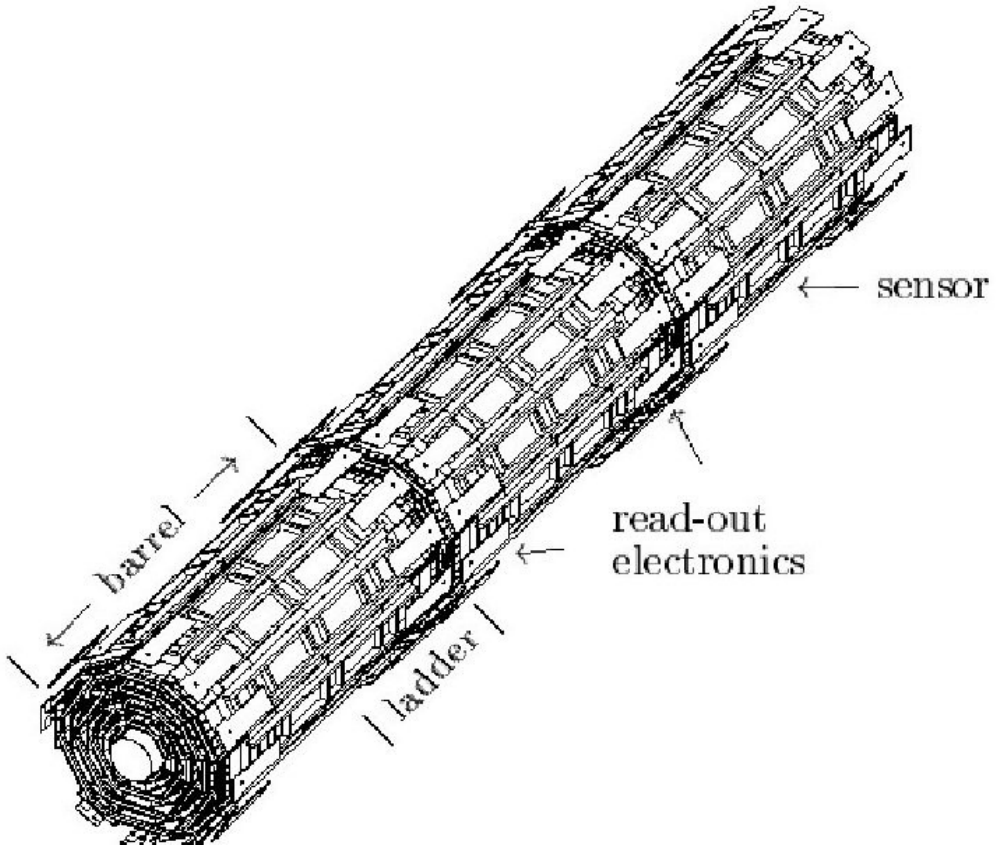

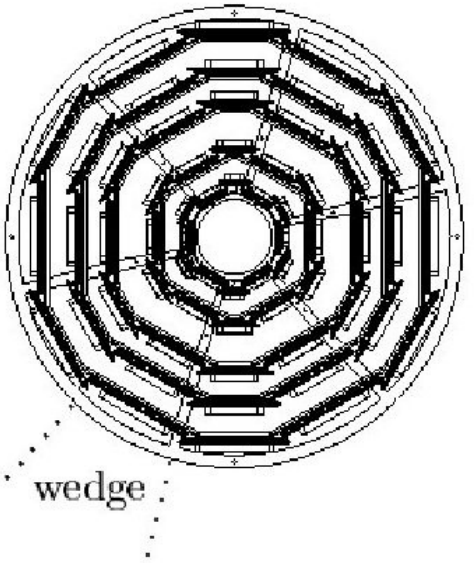

SVXII: the readout is
used in the trigger too

The Silicon Detectors: ISL

ISL detail

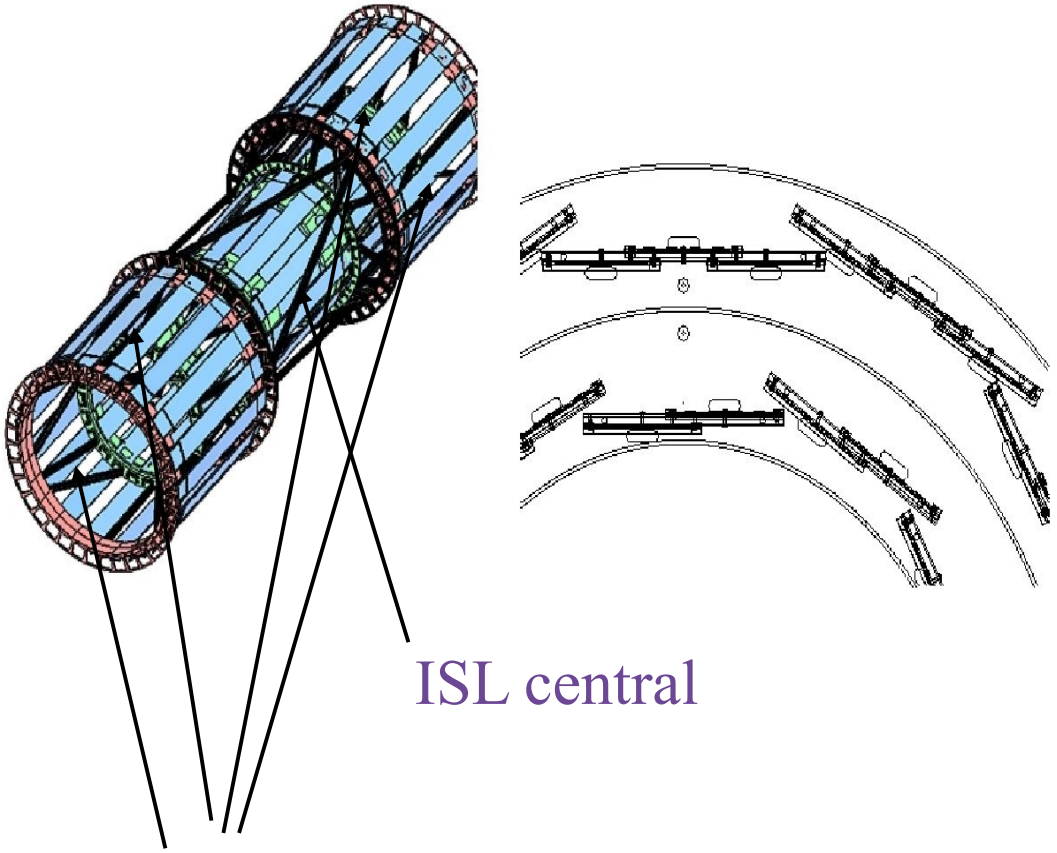

ISL central

ISLforward:
(inner and external barrels)

Radiation Field inside the detector

CDF Radiation Field

- Measured using more than 1000 thermo-luminescent dosimeters (TLDs)

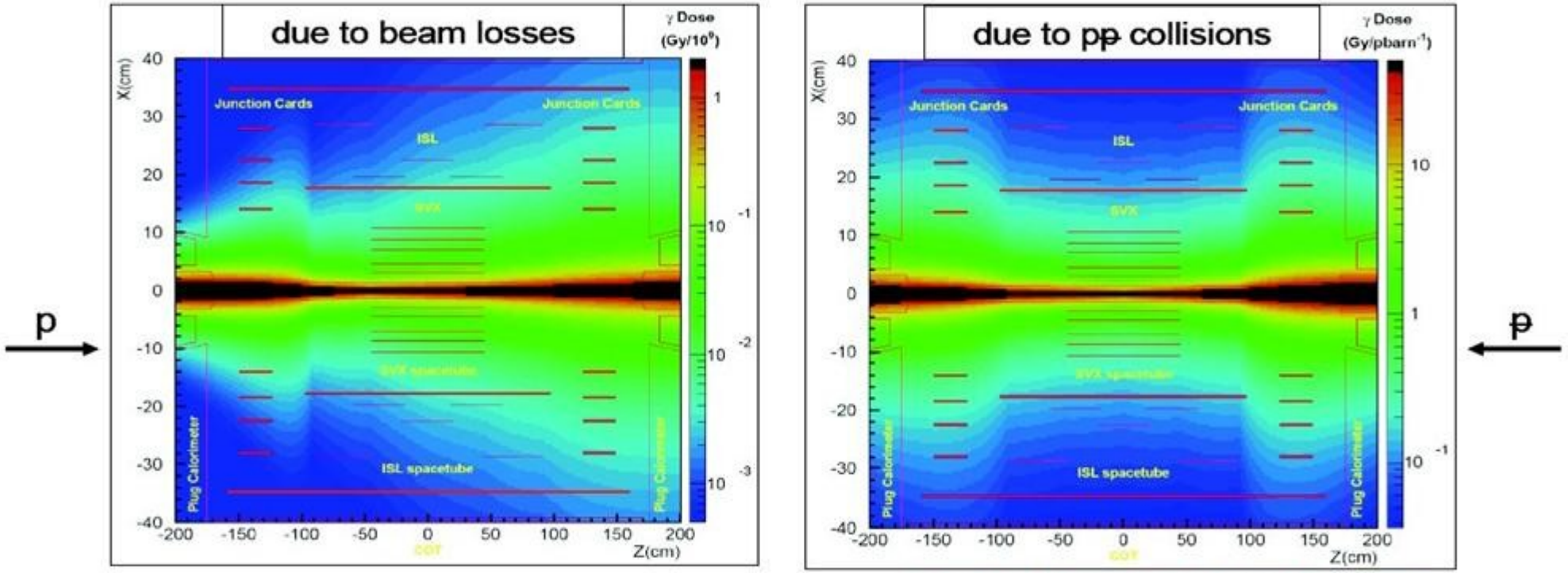

(See R. J. Tesarek *et al.*, IEEE NSS 2003)

- Radiation field is collision-dominated (> 90%)

Radiation damage

- **Two general types of radiation damage to the sensors:**
  - **Crystal damage** due to Non-Ionizing Energy Loss (NIEL): displacement damage, crystal defects.
    - increase of shot noise, change of effective doping concentration, increase of charge carrier trapping.
  - **Surface damage** from Ionizing Energy Loss (IEL) causing accumulation of charge in the SiO2 and the Si/SiO2 interface.
    - Inter-strip capacitance , breakdown behavior etc.

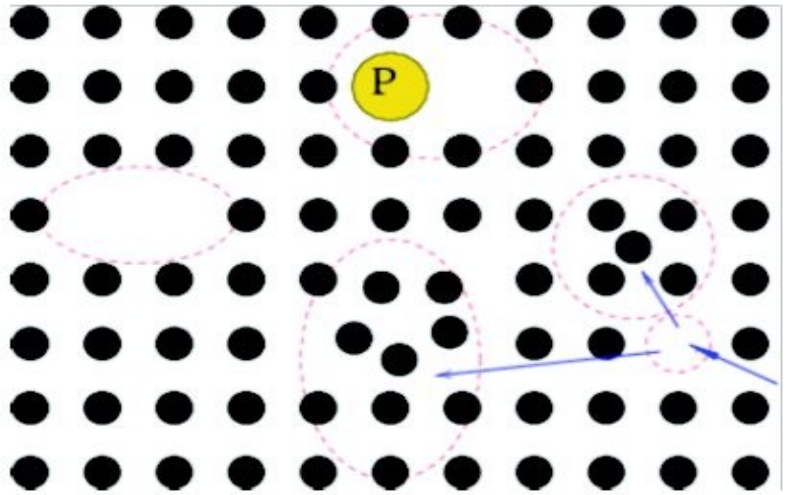

Crystal damage to the sensors is the main concern for detector longevity

Aging studies: variables of interest

- **Information on integrated radiation dose in a sensor is obtained from:**
  - ✓ **evolution of bias current:** provides "direct" information on the crystal condition, due to increase in leakage current. Change in leakage current is linear with the absorbed dose $\Delta I_{leak} = \alpha \Delta \Phi_{eq}$ (α measured in 2004 to be **1.65 ± 0.12**)
  - ✓ **evolution of depletion voltage:** gives information on our ability to deplete the sensors in the future. Its extrapolation predicts the need to raise applied bias voltage and its limit.
  - ✓ **Signal-over-noise (S/N) studies:** provide estimates of usability of the detector in charged particle tracking and in turn for physics analyses.

Depletion Voltage

- **Depletion voltage is the bias voltage required to get rid of free carriers in the bulk of the detector.**
- **The expected evolution depends on the dose (Hamburg Model):**
- **Before type inversion the depletion voltage decreases due to the reduction in the amount of free carriers**
- **After type inversion, depletion voltage steadily increases.**

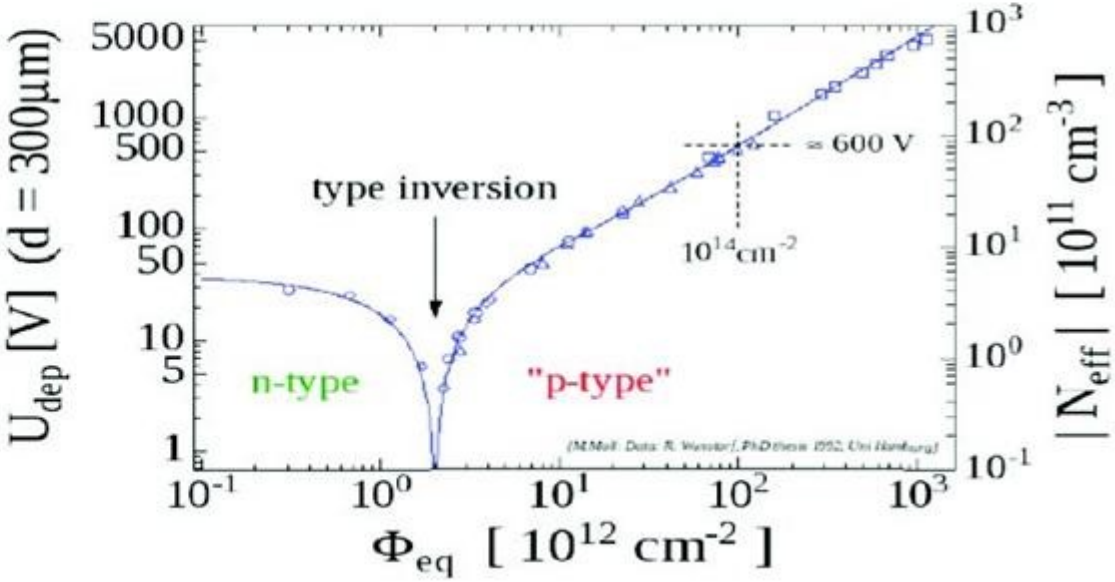

M.Moll, *PhD Thesis, (1992) UniHamburg*;

Sensor can operate while the Bias Voltage is below the Breaking Voltage

Depletion voltage Measurement

- **From charge (signal) collection efficiency:**
  - Charge collection is proportional to the depleted volume
  - Fully depleted sensor ➔ charge collection efficiency saturates
  - Extracted track residual information

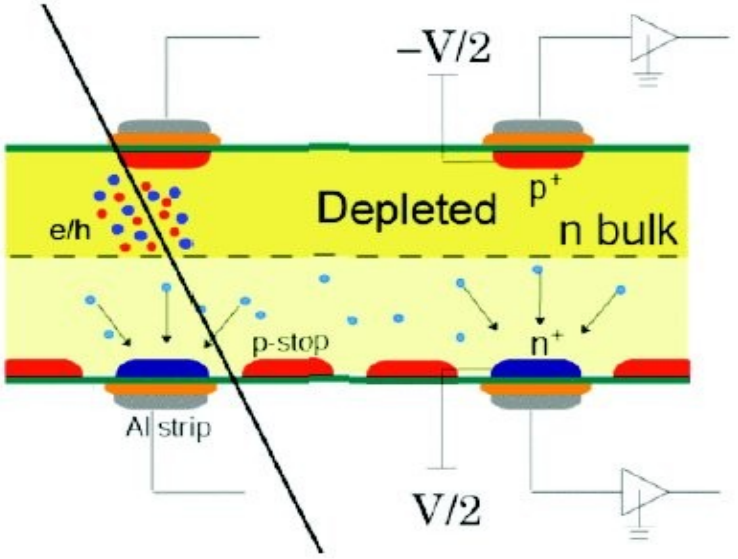

- **From noise at the n-side:**
  - Thermal noise from free carriers on the n-side is reduced with depletion (on the p-side)

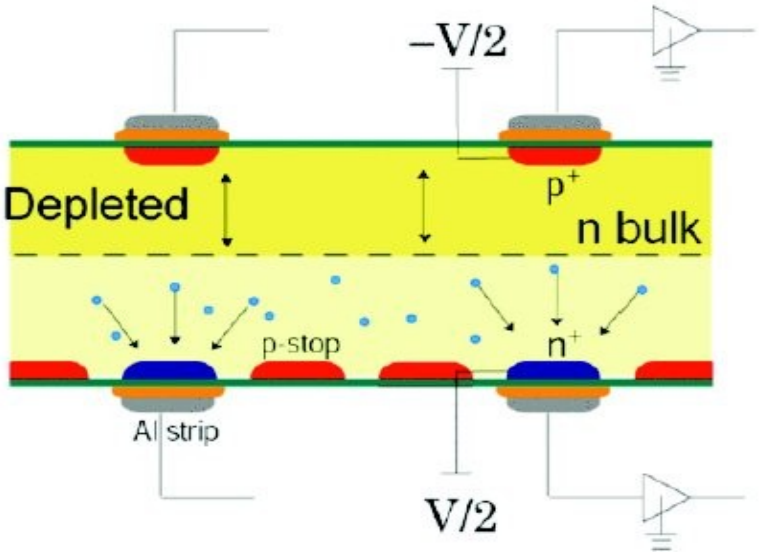

Depletion Voltage study – Signal Vs. Bias

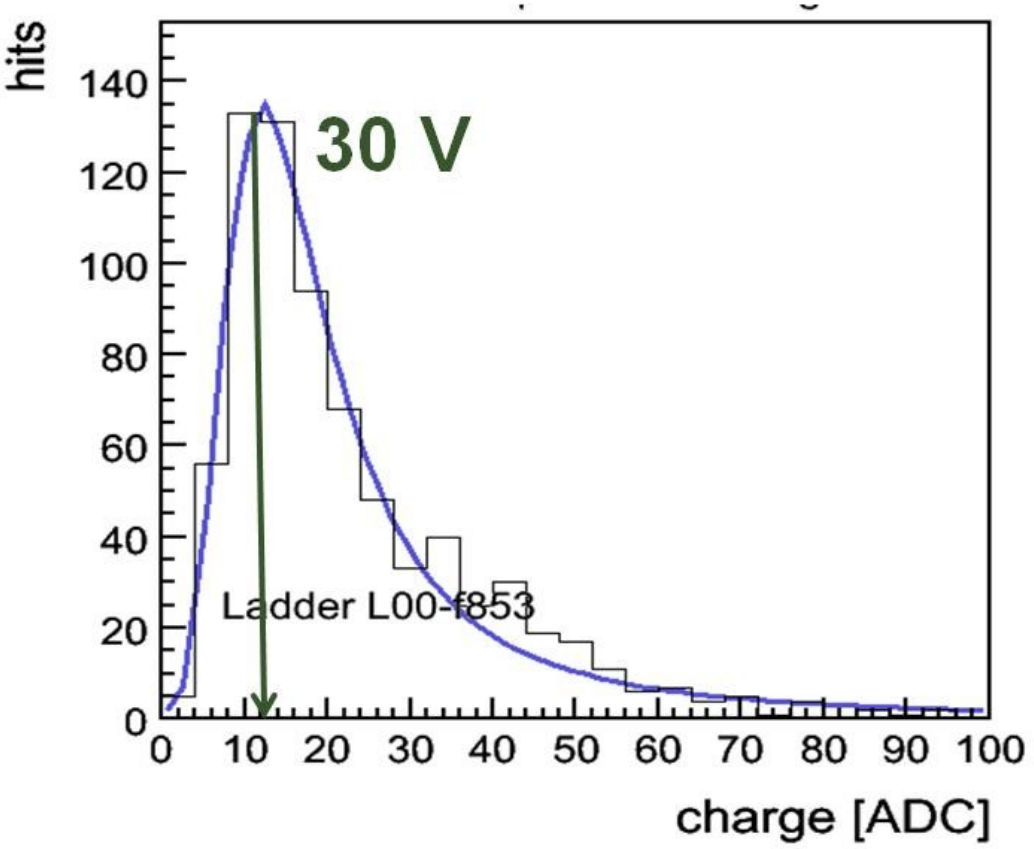

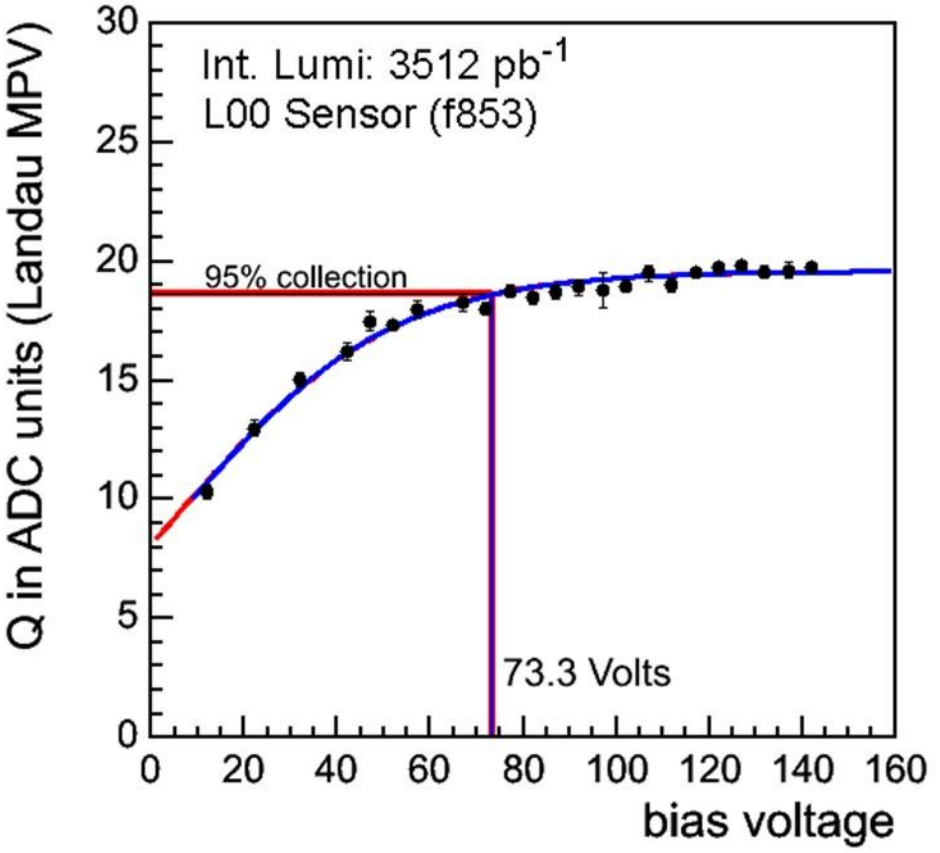

Depletion Voltage study – Signal Vs. Bias

- Plot charge for different bias voltages
- Define depletion voltage, V_d , as voltage that collects 95% of the charge at the plateau

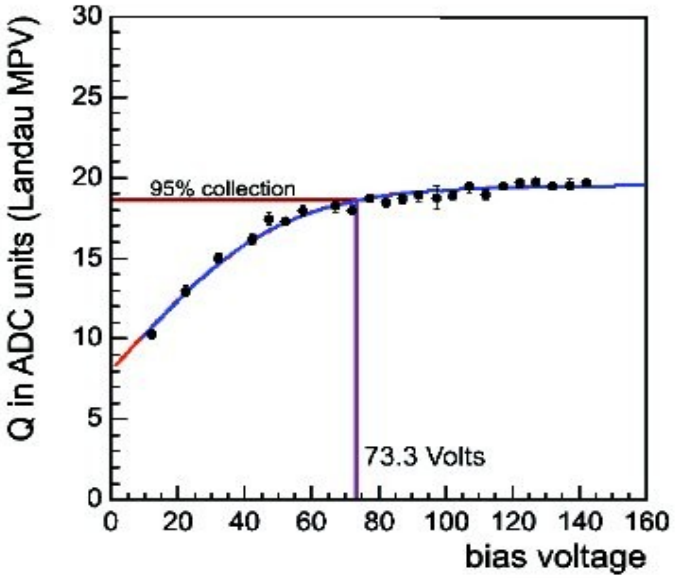

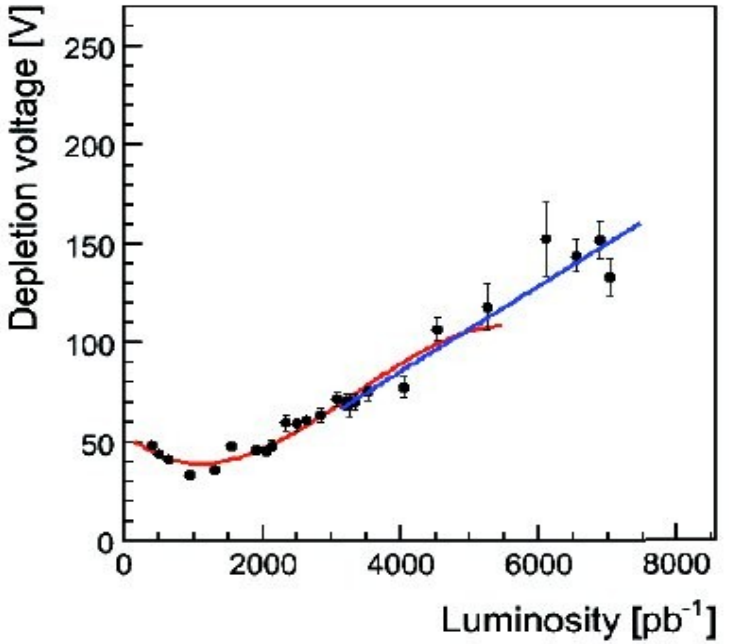

- Depletion Voltage as a function of integrated luminosity
  - 3rd order polynomial fit around the inversion point
  - Linear fit to extrapolate to the future

Depletion Voltage Projections L00-L0

Prediction for L00

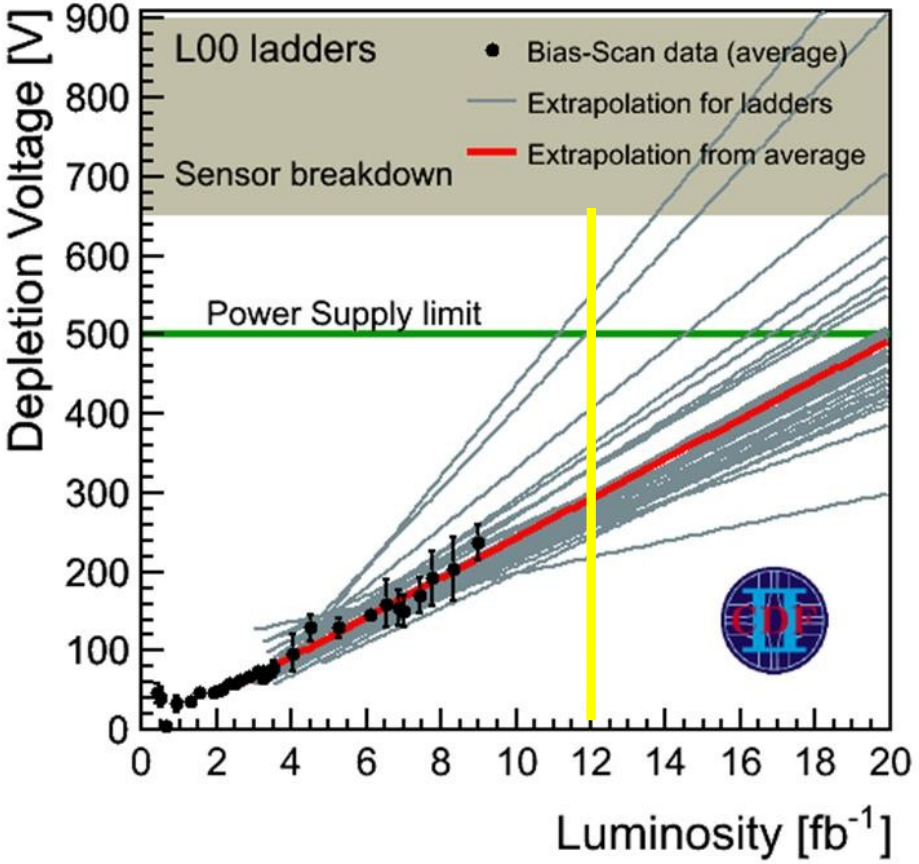

Prediction for SVX-L0

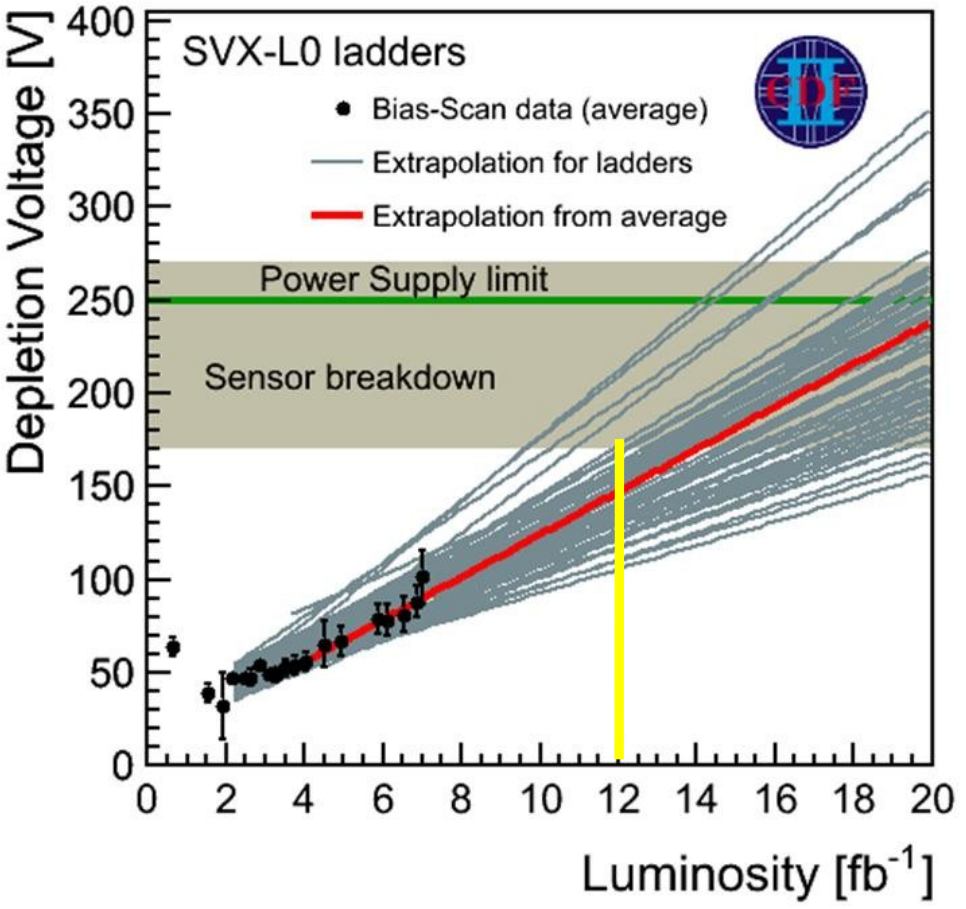

Very preliminary result on L00

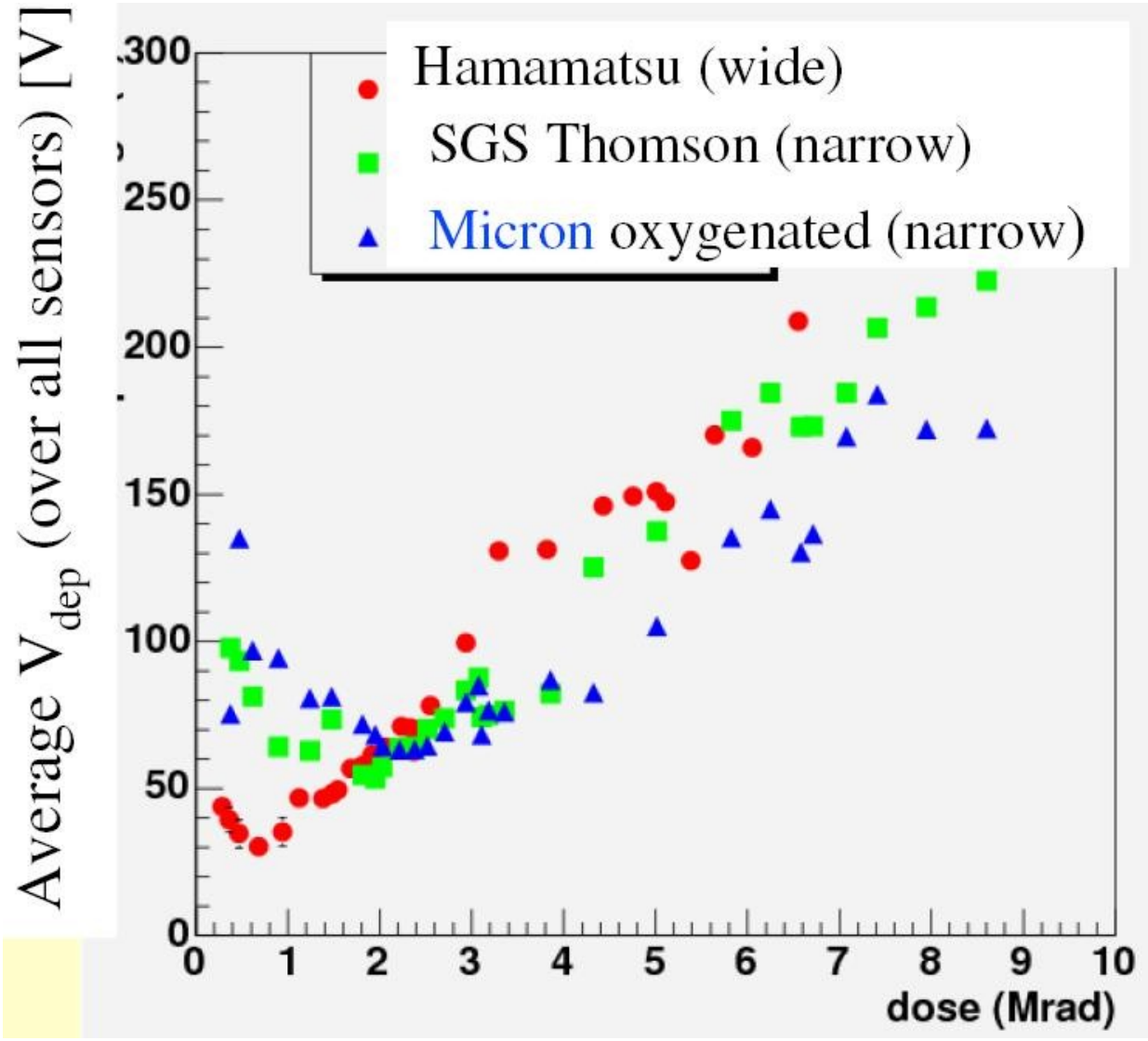

Studies still ongoing

Depletion Voltage study Noise Vs. Bias

Noise vs Bias Method

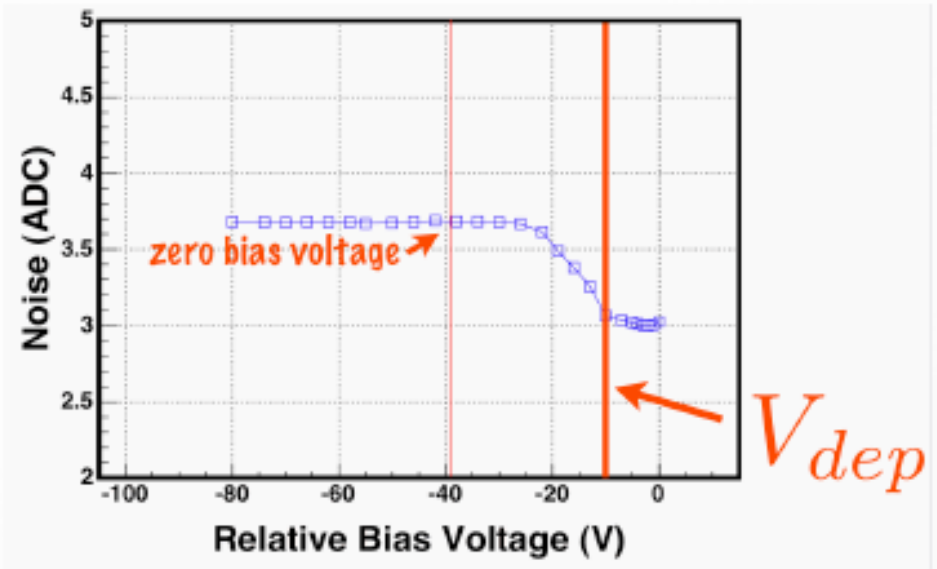

Find average dnoise vs bias voltage

Depletion voltage taken as interpolation to 104% of minimum value

GOOD: does not require beam time

BAD: not possible for single side strip or after inversion type

Signal / Noise projection

Signal from J/ψ → $\mu^+\mu^-$ tracks strip cluster charge,
Noise estimation from regular calibrations

r-phi

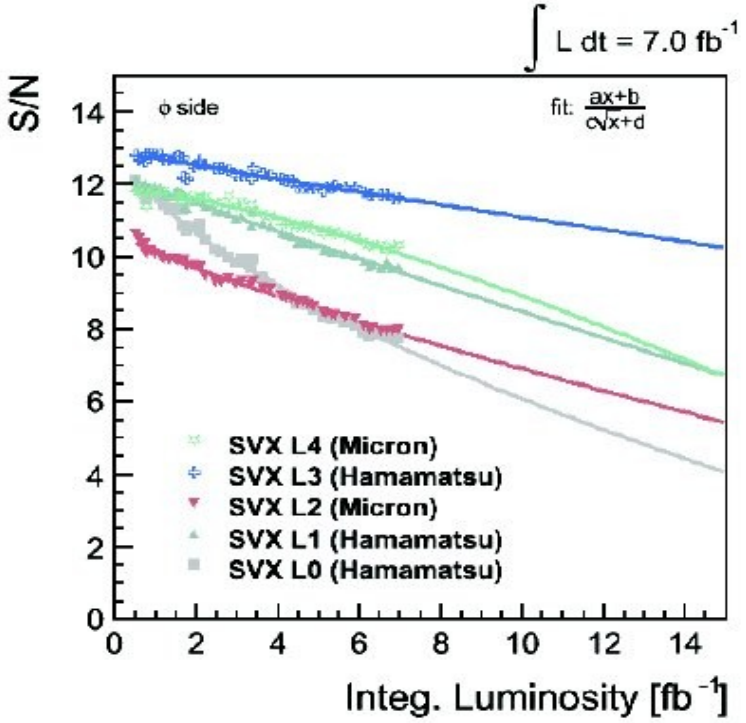

L00

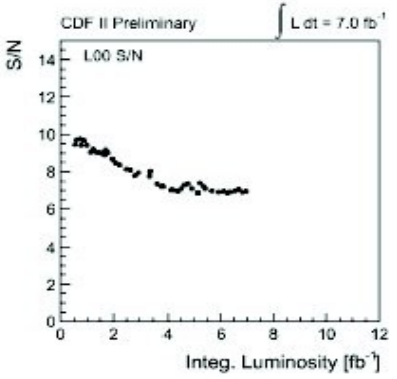

z

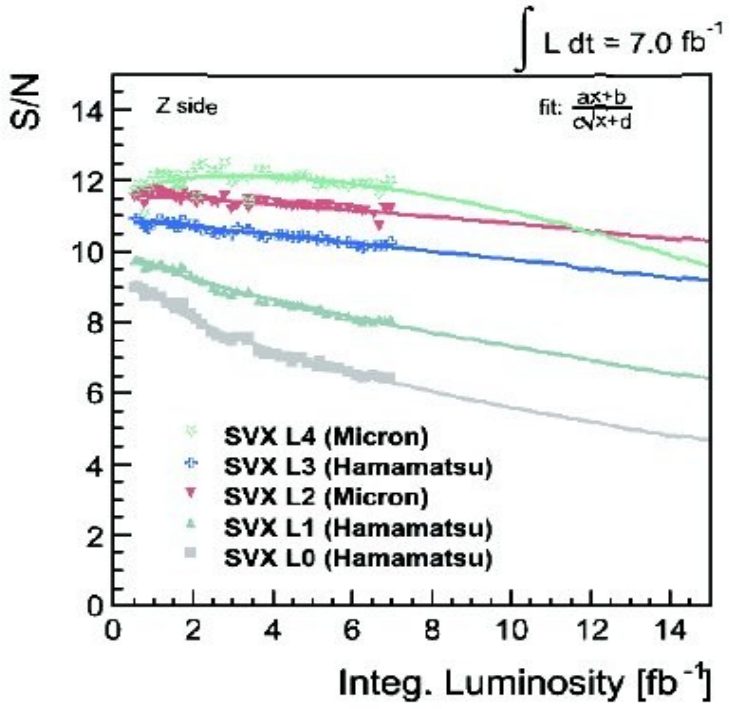

Not only the sensors are in a radiation environment

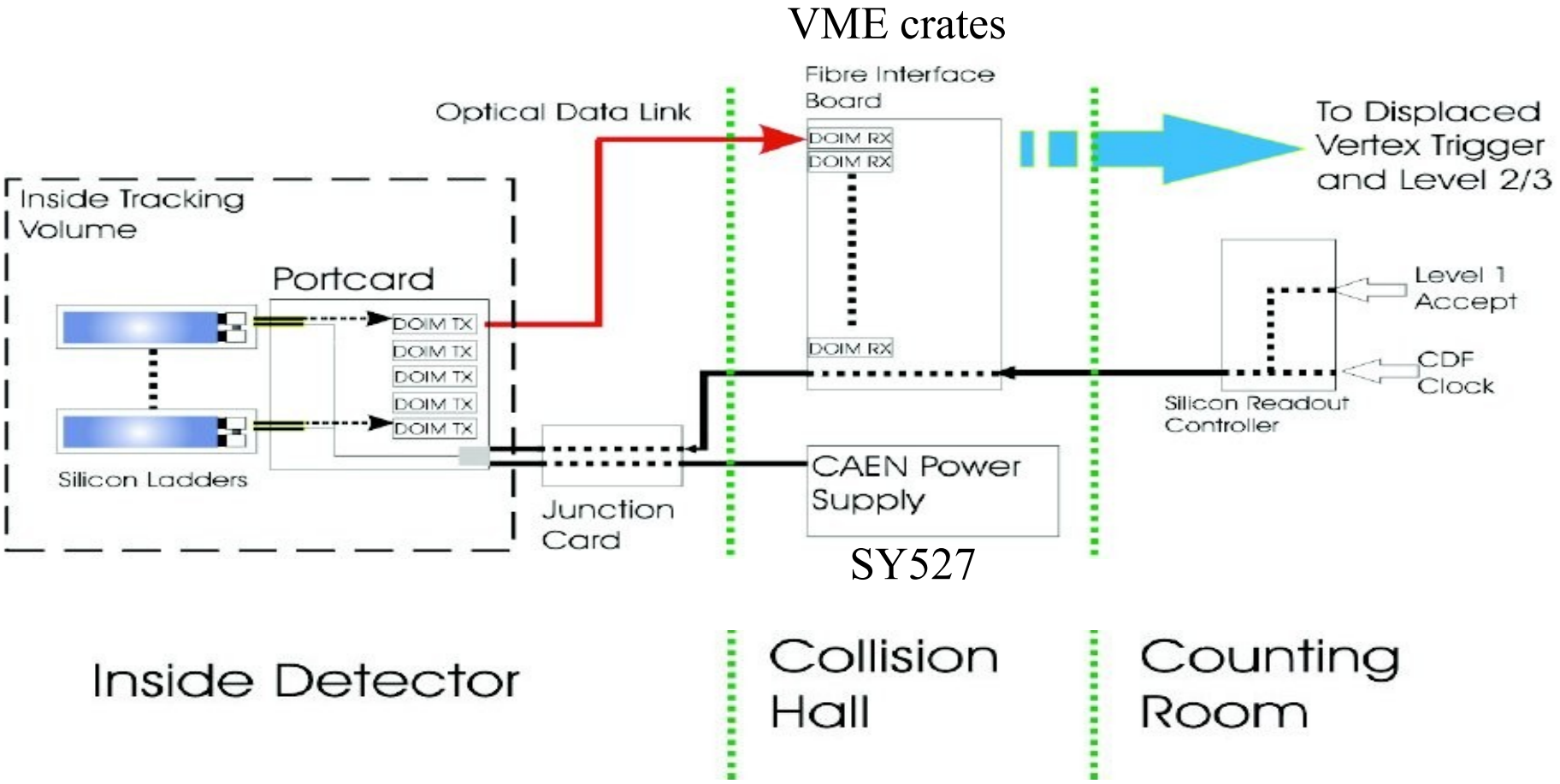

Main components:

Silicon Readout Controller (SRC): "brain" of the system

Fiber Interface Board (FIB): control signals and optical readout

Portcard: chip commands and optical transmitters (DOIMs)

Problems induced by trigger rates:

Wirebond Resonances:

- Observed loss of data & power to *z* sides of ladders
  - Found to correlate with high trigger rates
- Failure due to wirebond resonances
  - Wires orthogonal to magnetic field
  - Wires feels Lorentz force during readout
  - If frequency is right, wires resonate and break

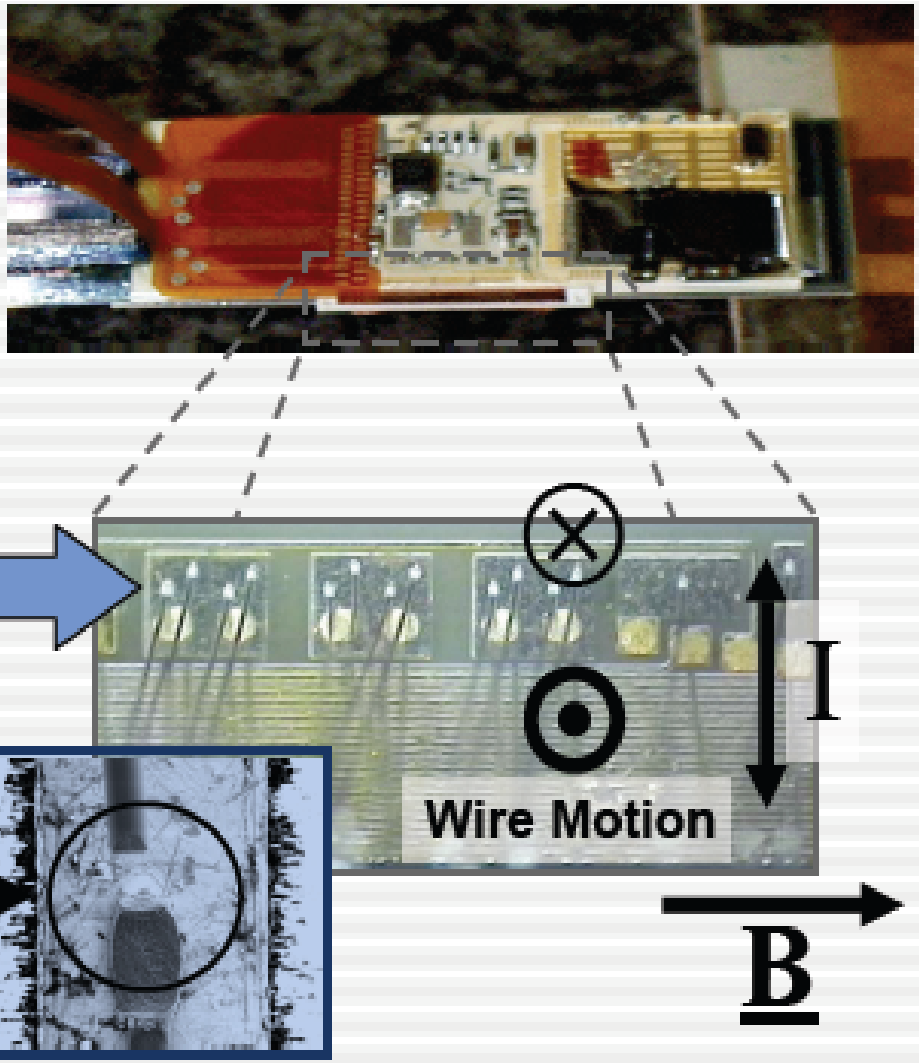

Other Operational Challenges

- **CAEN SY527 Power Supplies**
  - -Communication loss, corrupted read-back, spontaneous switch off,leaking capacitors
  - -A significant fraction of the supplies has been repaired

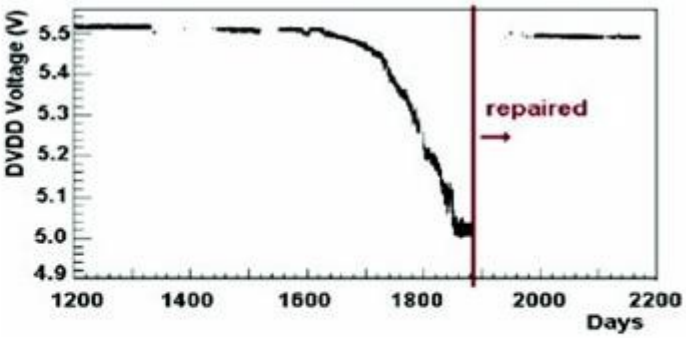

- **ISL Cooling Repairs**
  - -Glycol-water mix turned acidic causing corrosion.
  - -Repairs are challenging, access is possible only from inside the cooling conduits.
  - -Repairs during the 2007 and 2009 shutdowns have significantly improved the tightness of the system

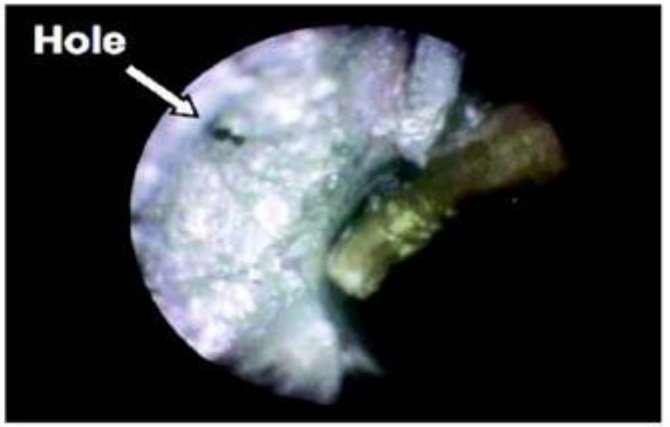

- **Spare electronic components… etc.,etc.**

Conclusions

- The CDF Run II silicon detectors are in good health after 10 years of operation.
- The inner layers have long progressed through inversion and exhibit consistent post-inversion behavior.
- Most ladders in SVX-L0 and SVX-L1 layers and the rest of the detector are expected be operable with high efficiency to 12 fb^{-1}
- L0 will begin to be affected beyond that point, which does not affect our b-vertex detection efficiency significantly.

Back-up slides

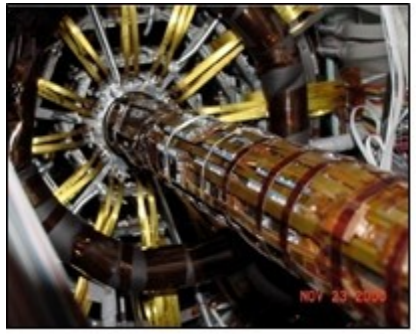

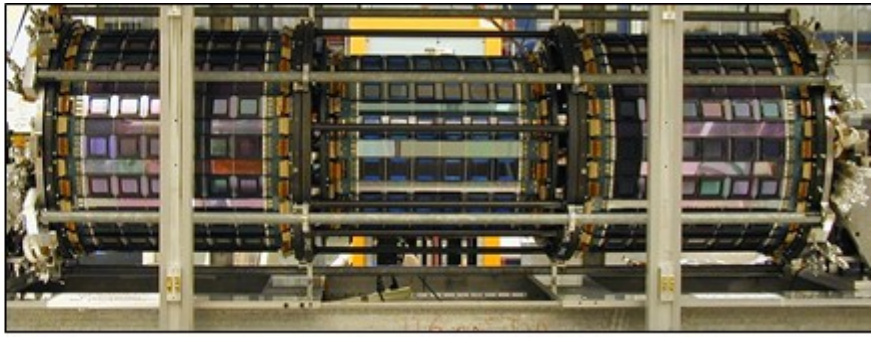

Measured Radiation Field

- Radiation field measured with TLDs outside the silicon volume in 2002-2003.
- NIM A514 188 (2003)
- Bias current evolution 2002-2004 consistent with this radiation dose

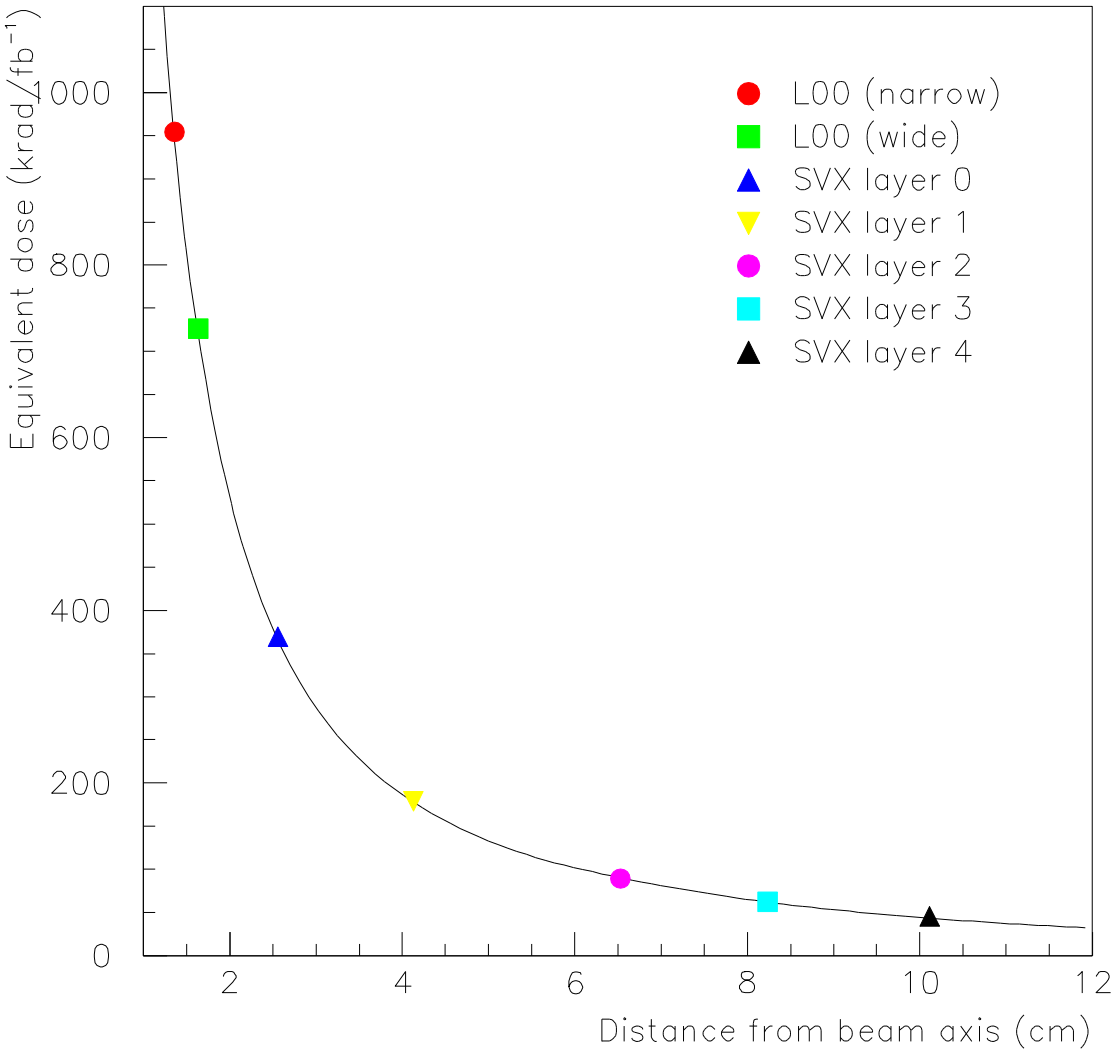

Inversion point

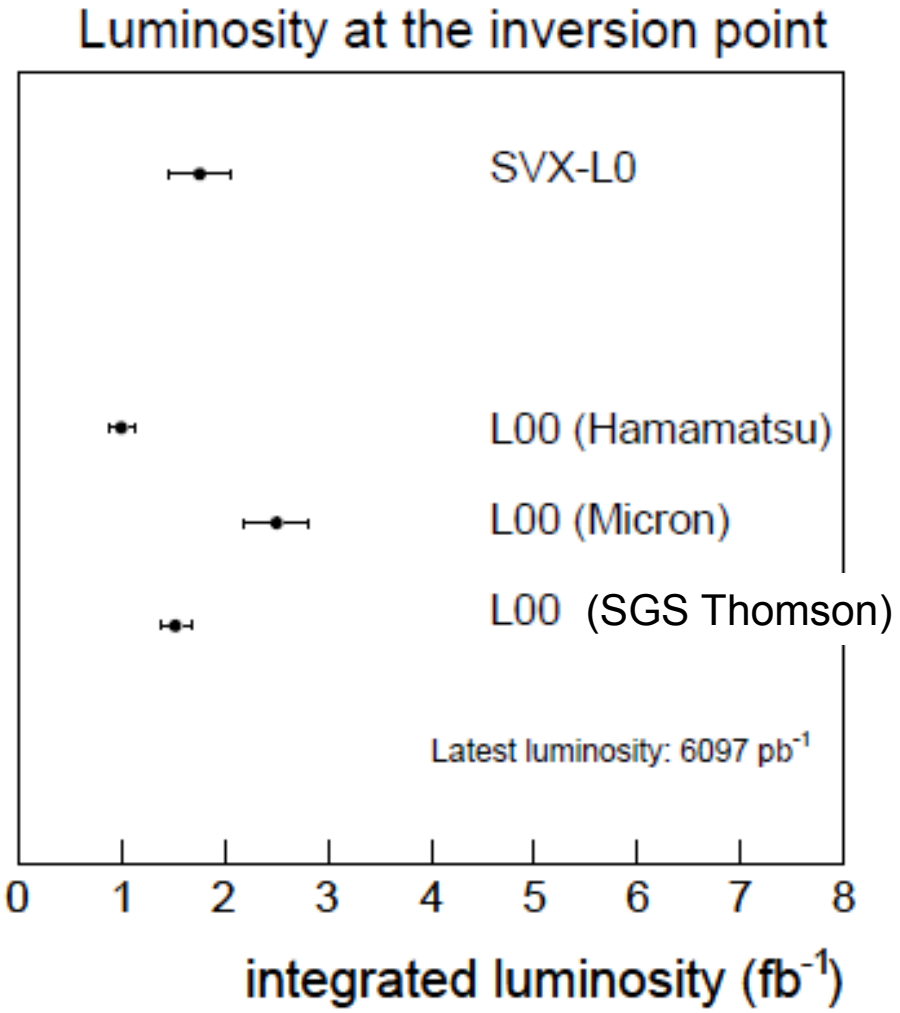

Silicon D.A.Q. for SVX II

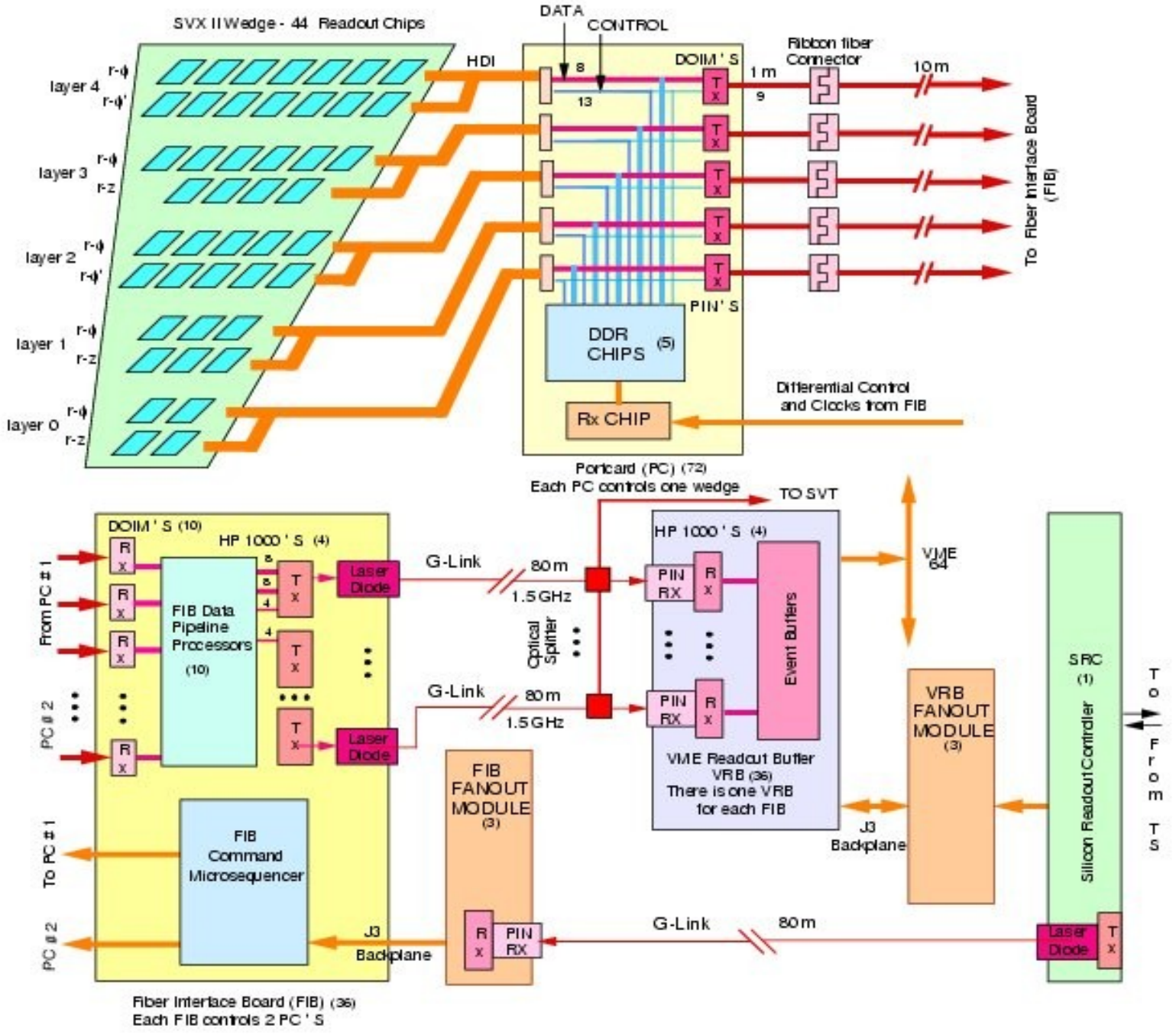

Evolution of Bias currents

- **Fluence in the CDF detector volume is dominated by the physics collisions - related to the delivered luminosity. . Measured using TLDs** (R. J. Tesarek et al. NSS 2003)

- **The fluence – integrated luminosity relationship depends on distance of the sensor to the beam, and is computed by extracting the fluence from the change in bias current.**

- **Using a 95 pb^{-1} data sample collected in 2004, a damage factor of 1.65 ± 0.12 was extracted from bias current data (P. Dong et al. CDF/7275).**

- **Bias evolution and TLD measurements agree well**

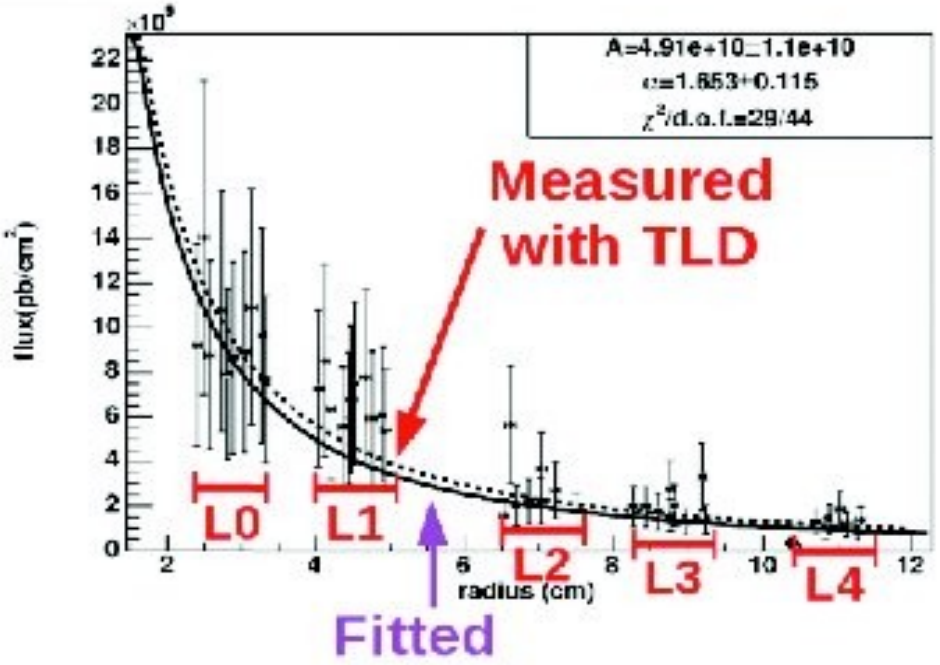

Depletion Voltage

Bias Scan Methods

Vary bias voltage and watch

- signal collection
- dnoise from n side strips

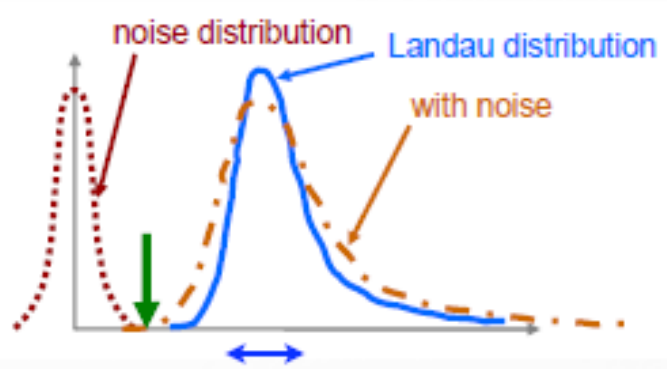

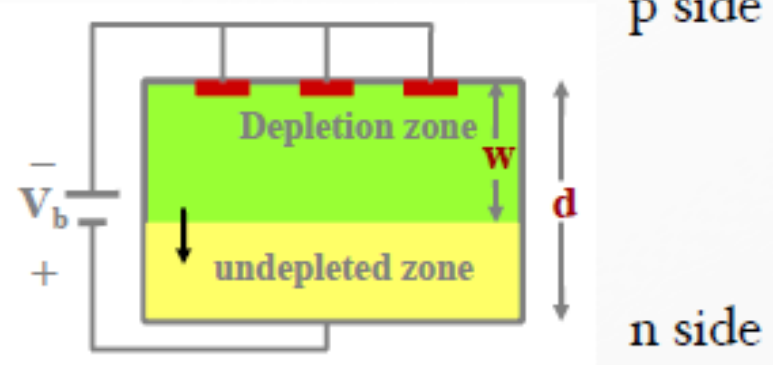

Depletion Voltage Projection L1

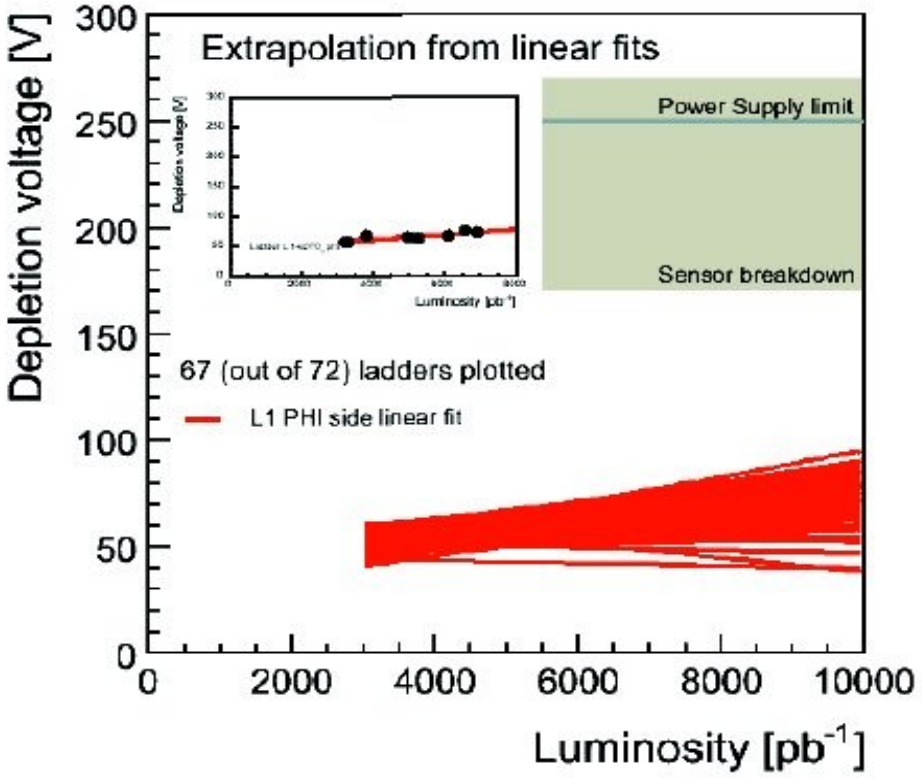

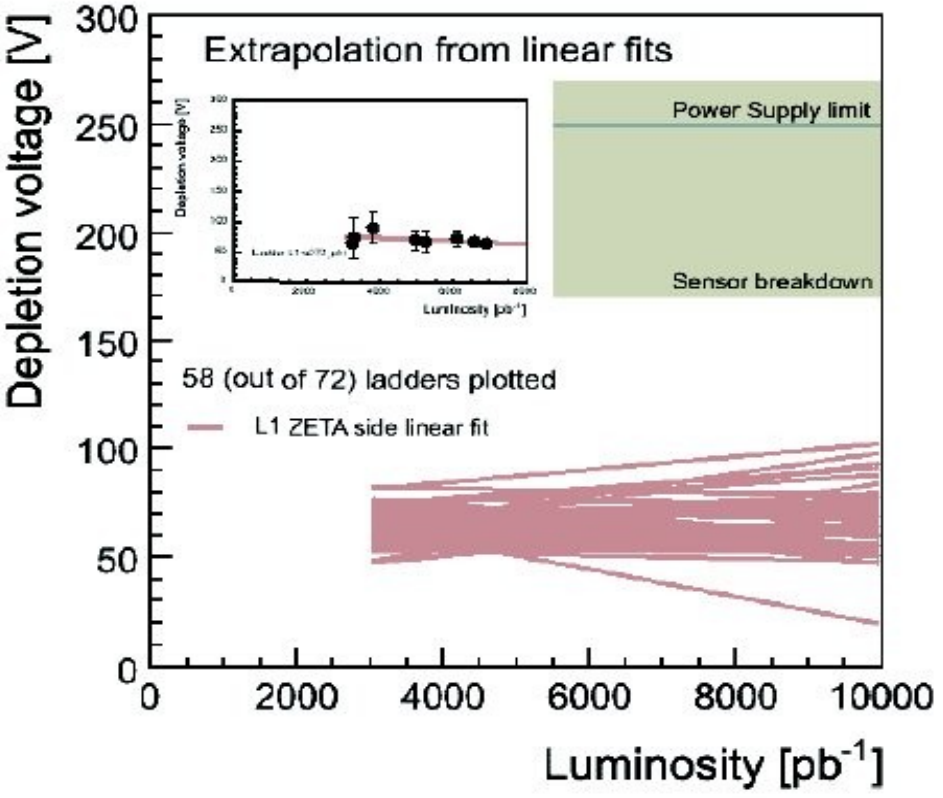

ISL cooling lines

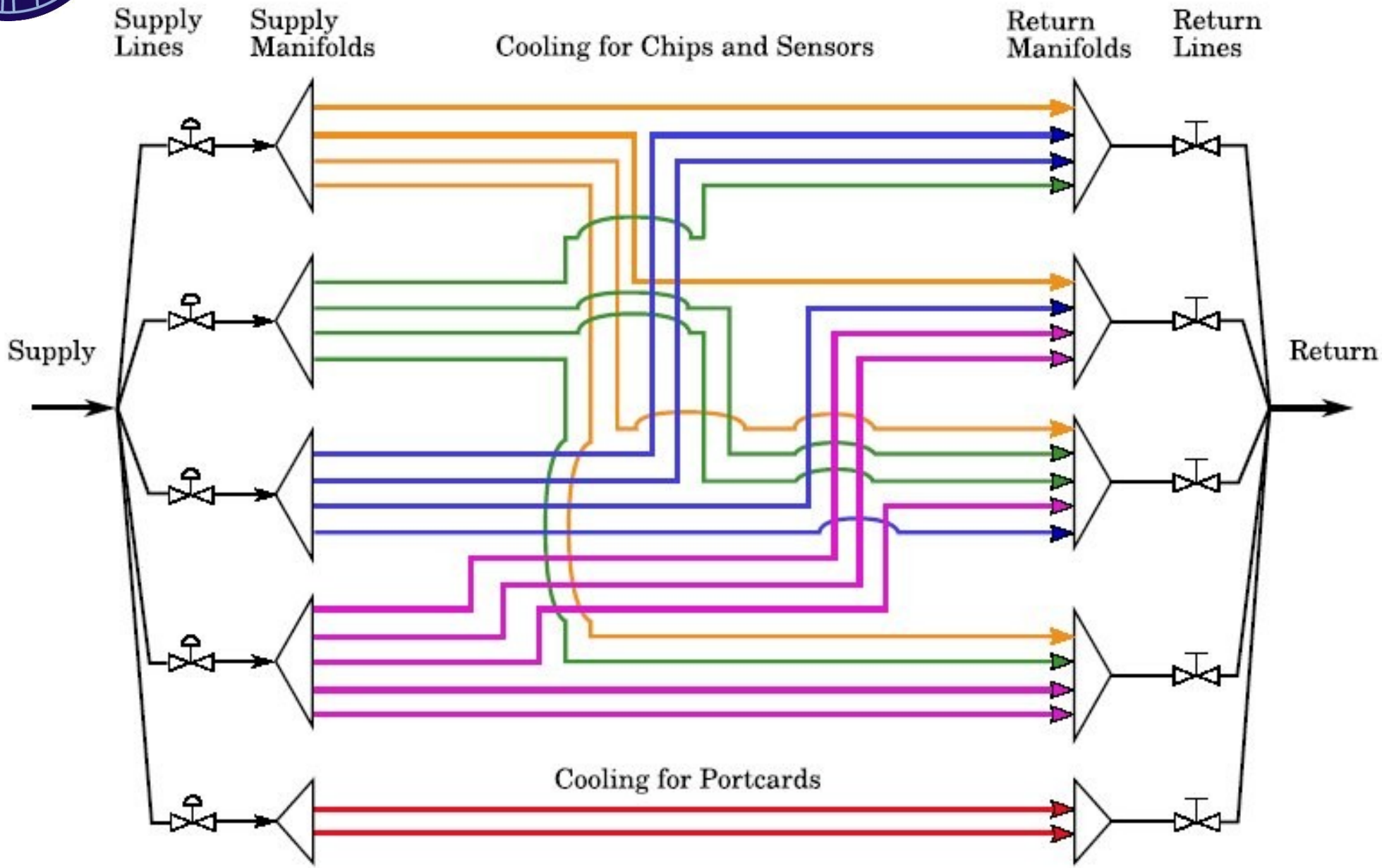

	SVX II	ISL
Detectors	720	900
Half ladders	360	300
Chips	3168	2100
Channels	405,504	268,800
Hybrids	720	300
Port Cards	72	30

SVXII.

Property	Layer 0	Layer 1	Layer 2	Layer 3	Layer 4
number of ϕ strips	256	384	640	768	896
number of Z strips	256	576	640	512	896
number of ϕ chips	2	3	5	6	7
number of Z chips	2	3	5	4	7
stereo angle	90^o	90^o	$+1.2^o$	90^o	-1.2^o
ϕ strip pitch (μm)	60	62	60	60	65
Z strip pitch (μm)	141	125.5	60	141	65
total width (mm)	17.140	25.594	40.300	47.860	60.170
total length (mm)	74.3	74.3	74.3	74.3	74.3
active width (mm)	15.300	23.746	38.340	46.020	58.175
active length (mm)	72.43	72.43	72.38	72.43	72.38
number of detectors	144	144	144	144	144

Table 5.3: Silicon detector mechanical dimensions

Table 1: Summary of L00, SVXII and ISL basic parameters.

Name	Radius (cm)	Orientation	manufacturer
L00 (narrow)	1.35	$r\phi$	SGS Thomson, Micron
L00 (wide)	1.62	$r\phi$	Hamamatsu
SVX L0	2.54	$r\phi$,z	Hamamatsu
SVX L1	4.12	$r\phi$,z	Hamamatsu
SVX L2	6.52	$r\phi$,1.2^o	Micron
SVX L3	8.22	$r\phi$,z	Hamamatsu
SVX L4	10.10	$r\phi$,1.2^o	Micron
ISL L6 Central	22.00	$r\phi$,1.2^o	Hamamatsu
ISL L6 Fwd/Bwd	20.00	$r\phi$,1.2^o	Hamamatsu
ISL L7 Fwd/Bwd	28.00	$r\phi$,1.2^o	Micron

Laser diode/photo diode

Laser Diode	
1550nm InGaAsP/InP edge emitting laser diode	
Wavelength	1550 nm nominal
Bias Current	20 mA
Threshold Current	10 mA
Optical Power	$\geq$ 200 mW coupled to fiber
Forward Voltage	1 V
Operating Temperature	0–40 (°C)

Table 5.10: Characteristics of laser diode

Photo Diode	
Description: InGaAs/InP planar PIN	
Sensitive Wavelength	1000–1605 nm
Responsivity (A/W)	0.9 @1550 nm
Dark Current (nA)	$\leq$ 1.5 @-5V 25°C
Capacitance (pf)	$\leq$ 4
Breakdown Voltage	15 V
Bandwidth (GHz)	1.9 @3dB
Operating Temperature	0–40 °C

Table 5.11: Characteristics of photodiode

Driver Chip	
Input	Differential with common mode voltage 2.5 ± 0.5 V and differential swing greater than 100 mV
Data rate	53 MHz
Switching time	$t_r, t_f \leq 1.5$ ns
Channel skew	$< 1ns$
Supply Voltage	5 V
Control input	TTL signal to disable driver
Power dissipation	< 2.3 mW

Table 5.12: Characteristics of driver circuit

Receiver Chip	
Output	ECL
Data rate (MHz)	53
Switching time (ns)	$t_r, t_f \leq 2.0$
Channel skew (ns)	< 1
Supply Voltage (V)	5
Power dissipation (mW)	< 2.0

Table 5.13: Characteristics of receiver circuit

Detector Parameter	SVX′	SVX II
Readout coordinates	r-ϕ	r-ϕ; r-z
Number of barrels	2	3
Number of layers per barrel	4	5
Number of wedges per barrel	12	12
Ladder length	25.5 cm	29.0 cm
Combined barrel length	51.0 cm	87.0 cm
Layer geometry	3° tilt	staggered radii
Radius innermost layer	3.0 cm	2.44 cm
Radius outermost layer	7.8 cm	10.6 cm
r-ϕ readout pitch	60;60;60;55 μm	60;62;60;60;65 μm
r-z readout pitch	absent	141;125.5;60;141;65 μm
Length of readout channel (r-ϕ)	25.5 cm	14.5 cm
r-ϕ readout chips per ladder	2;3;4;6	4;6;10;12;14
r-z readout chips per ladder	absent	4;6;10;8;14
r-ϕ readout channels	46,080	211,968
r-z readout channels	absent	193,536
Total number of channels	46,080	405,504
Total number of readout chips	360	3168
Total number of detectors	288	720
Total number of ladders	96	180

Table 5.1: Comparison of SVX′ and 5-layer SVX II.

ISL

	Atlas	Atlas	L3	L3	Delphi	Delphi	ISL	ISL
side	n	n	p	n	n	n	p	n
S/N	11	17	15	15	12	21	>12	12
RP (μm)	112	112	50	150	100	50	110	146
SP (μm)	56	56	25	50	100	50	55	73
SP/$\sqrt{12}$	16.0	16	7.2	14.4	28.0	14.4	16.0	21.0
σ (μm)	15.6	12.9	7.0	15.0	23.0	10.0	<16.0	<23.0

Table 6.2: Comparison to other silicon detectors with alternate strip readout.

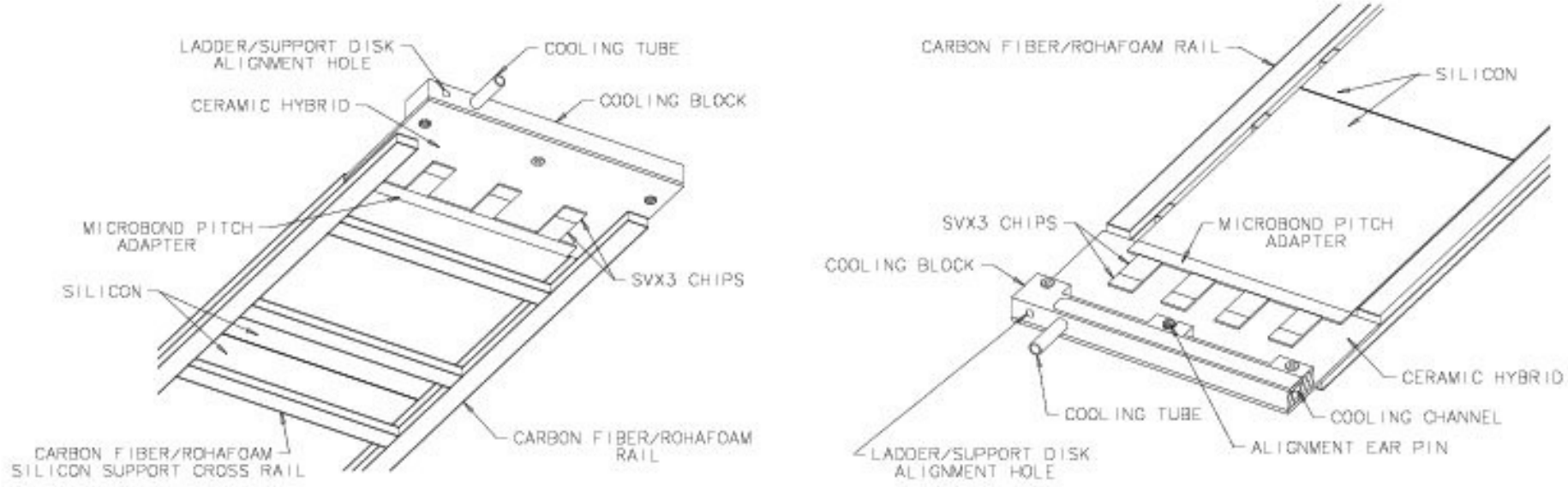

Figure 6.4: A close up view of the readout hybrid on the stereo side of a ladder (left) and the readout hybrid and cooling channel on the axial side of a ladder (right).

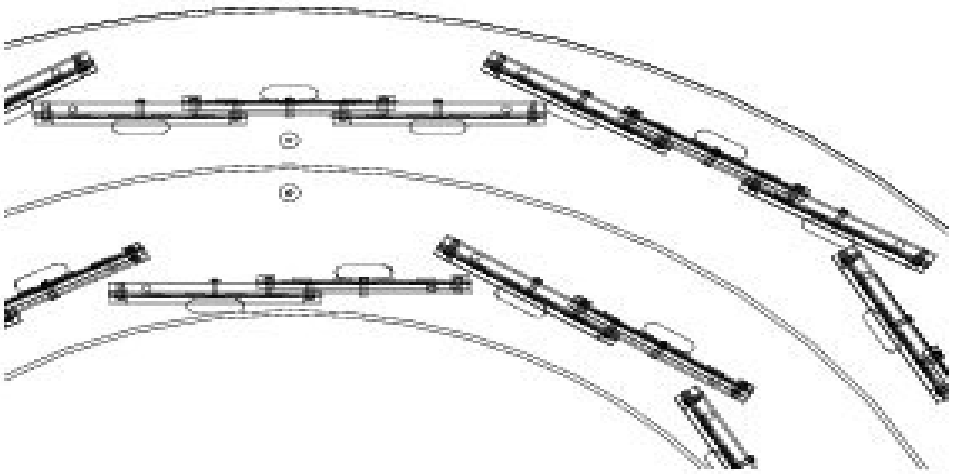

Figure 6.6: Closeup of one section of the end view of an endplug barrel.

ISL

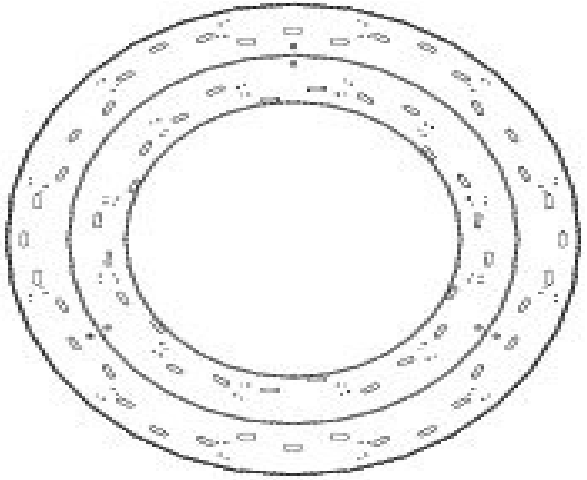

Figure 6.7: Carbon fiber support disks.

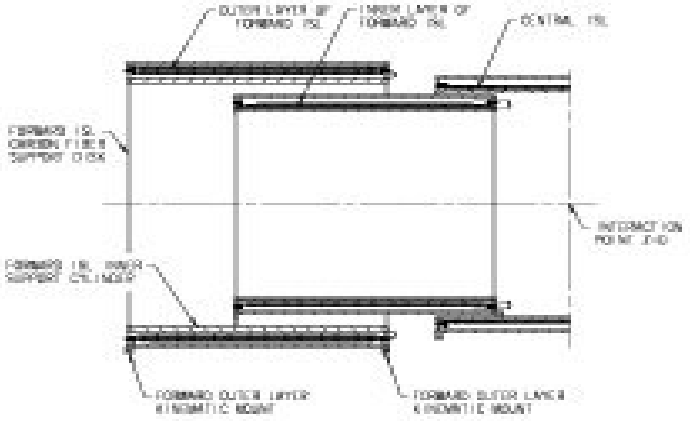

Figure 6.8: Schematic view of the ISL system.

Readout Chip Accounting

Some of the common failure modes:

- Detector = Port-cards, Junction Cards, cables, and sensors issues.
- Optical = errors from the TX data transmitters in the port-cards
- Jumper failures = chip damage due to resonances
- AVDD2 = a SVX3D chip failure mode caused by thermal cycles

END